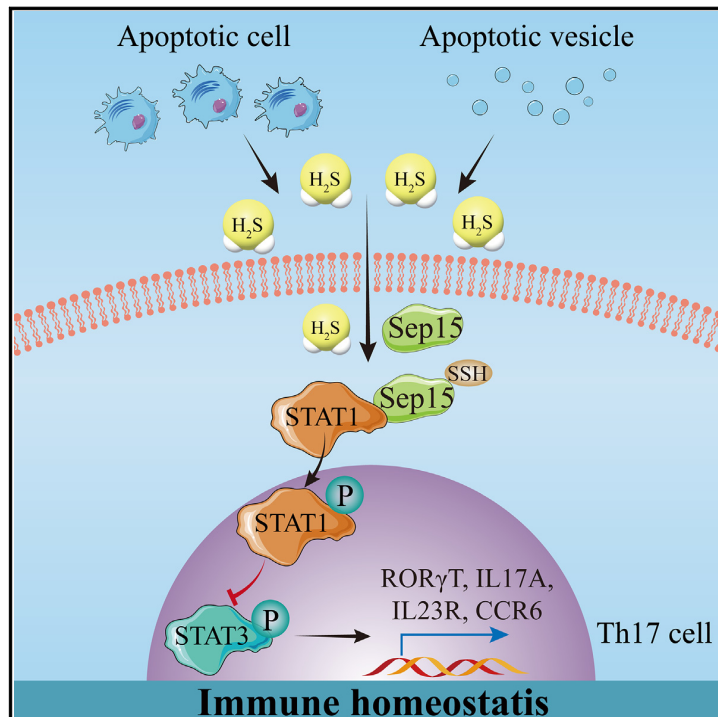


Cell Metabolism

Apoptosis releases hydrogen sulfide to inhibit Th17 cell differentiation

Graphical abstract



Authors

Qianmin Ou, Xinhua Qiao,
Zhengshi Li, ..., Xiaoxing Kou,
Chang Chen, Songtao Shi

Correspondence

changchen@ibp.ac.cn (C.C.),
shisongtao@mail.sysu.edu.cn (S.S.)

In brief

H₂S is an important endogenous regulator of the immune system. Ou et al. demonstrate that apoptotic cells and vesicles produce H₂S to maintain immune homeostasis and inhibit Th17 cell differentiation via sulfhydrylation of Sep15^{C38}.

Highlights

- Apoptotic cells are an important resource providing endogenous H₂S
- Apoptotic-cell-generated H₂S maintains immune homeostasis
- H₂S inhibits the aberrant Th17 cell differentiation via sulfhydrylation of Sep15
- H₂S from apoptotic cells ameliorates murine systemic lupus erythematosus phenotypes



Article

Apoptosis releases hydrogen sulfide to inhibit Th17 cell differentiation

Qianmin Ou,^{1,7} Xinhua Qiao,^{2,7} Zhengshi Li,^{1,7} Luhan Niu,¹ Fangcao Lei,¹ Ruifeng Cheng,³ Ting Xie,² Ning Yang,⁴ Yao Liu,⁴ Ling Fu,³ Jing Yang,³ Xueli Mao,¹ Xiaoxing Kou,^{1,6} Chang Chen,^{2,5,*} and Songtao Shi^{1,6,8,*}

¹South China Center of Craniofacial Stem Cell Research, Hospital of Stomatology, Sun Yat-sen University, Guangdong Provincial Key Laboratory of Stomatology, Guangzhou 510080, China

²National Laboratory of Biomacromolecules, CAS Center for Excellence in Biomacromolecules, Institute of Biophysics, Chinese Academy of Sciences, Beijing 100101, China

³State Key Laboratory of Proteomics, Beijing Proteome Research Center, National Center for Protein Sciences (Beijing), Beijing Institute of Lifeomics, Beijing 100101, China

⁴Department of Pediatric Dentistry, School and Hospital of Stomatology, China Medical University, Shenyang 110002, China

⁵University of Chinese Academy of Sciences, Beijing 100049, China

⁶Key Laboratory of Stem Cells and Tissue Engineering (Sun Yat-Sen University), Ministry of Education, Guangzhou 510080, China

⁷These authors contributed equally

⁸Lead contact

*Correspondence: changchen@ibp.ac.cn (C.C.), shisongtao@mail.sysu.edu.cn (S.S.)

<https://doi.org/10.1016/j.cmet.2023.11.012>

SUMMARY

Over 50 billion cells undergo apoptosis each day in an adult human to maintain immune homeostasis. Hydrogen sulfide (H₂S) is also required to safeguard the function of immune response. However, it is unknown whether apoptosis regulates H₂S production. Here, we show that apoptosis-deficient MRL/lpr (B6.MRL-Fas^{lpr}/J) and Bim^{-/-} (B6.129S1-Bcl2l11tm1.1Ast/J) mice exhibit significantly reduced H₂S levels along with aberrant differentiation of Th17 cells, which can be rescued by the additional H₂S. Moreover, apoptotic cells and vesicles (apoVs) express key H₂S-generating enzymes and generate a significant amount of H₂S, indicating that apoptotic metabolism is an important source of H₂S. Mechanistically, H₂S sulfhydrates selenoprotein F (Sep15) to promote signal transducer and activator of transcription 1 (STAT1) phosphorylation and suppress STAT3 phosphorylation, leading to the inhibition of Th17 cell differentiation. Taken together, this study reveals a previously unknown role of apoptosis in maintaining H₂S homeostasis and the unique role of H₂S in regulating Th17 cell differentiation via sulfhydration of Sep15^{C38}.

INTRODUCTION

An adult human loses 50–70 billion cells each day due to apoptosis, which plays a pivotal role in the maintenance of tissue homeostasis.¹ Accumulating experimental evidence has shown that apoptotic disorders can cause a variety of anomalies, such as autoimmune disease, aging, and cancer.^{2,3} Apoptosis deficiency can promote the differentiation of inflammatory lymphocytes, which exacerbates the immune disorder and disease progress.^{4,5} However, the details of how apoptosis deficiency contributes to physiopathological processes of immune responses are not fully understood. Recent studies show that apoptotic cells can release metabolites to exert certain physiological functions.^{1,6}

Hydrogen sulfide (H₂S), an endogenous gasotransmitter, also plays a critical role in regulating tissue homeostasis.^{7–9} In mammals, H₂S is synthesized from L-cysteine through three enzymes, namely cystathionine β-synthase (CBS), cystathionine γ-lyase (CSE), and 3-mercaptopyruvate sulfurtransferase (3-MST).^{10,11} H₂S can induce cellular changes through a process

known as protein sulfhydration, which is a kind of protein post-translational modification.¹² By converting thiol –SH groups in the cysteine residues of target proteins to hydropersulfide –SSH groups, the structure and functionality of proteins can be modified.¹² Our previous study showed that endogenous H₂S is essential to maintain immune homeostasis, and H₂S deficiency has been linked to T cell-related immune disorders.¹³ Since both apoptosis deficiency and H₂S deficiency can lead to serious immune disorders, we hypothesize that the apoptosis process may be associated with endogenous H₂S production.

Apoptosis deficiency is closely linked to systemic lupus erythematosus (SLE), which presents with a significantly increased number of Th17 cells in the circulation and tissues.^{14,15} The infiltration of Th17 cells causes tissue inflammation and organ damage.^{16,17} Suppressing the differentiation and survival of Th17 cells in patients with SLE is a promising approach to alleviate inflammation injury and stall disease progress.¹⁴

Apoptotic vesicles (apoVs) are metabolic extracellular vesicles (EVs) released from apoptotic cells.¹⁸ ApoVs inherit various components from their parent cells, including DNA, RNA, proteins,



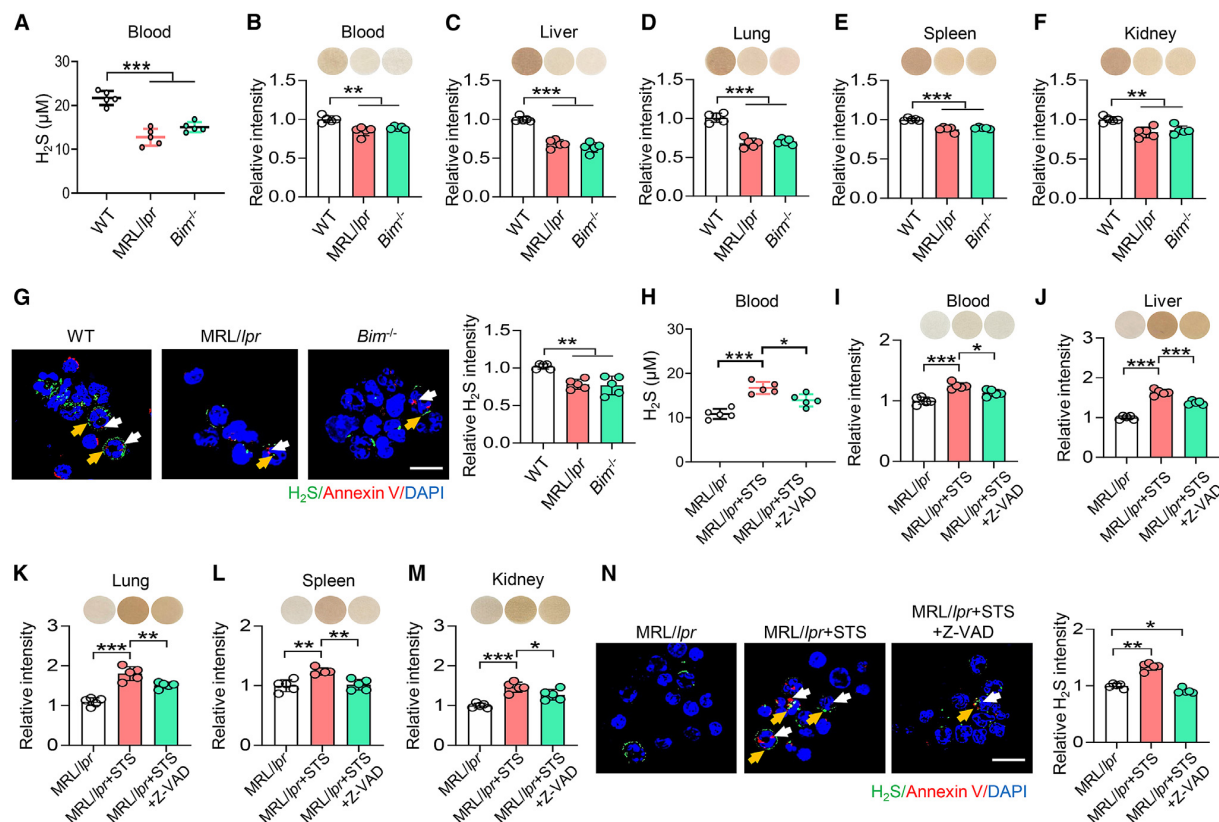


Figure 1. Apoptosis-deficient mice showed reduced H₂S levels

(A and B) H₂S microelectrode and lead acetate formation test showed that the blood H₂S concentration in female MRL/lpr and Bim^{-/-} mice was decreased; n = 5 per group.

(C–F) Lead acetate formation test revealed that the H₂S concentration in the liver, lung, spleen, and kidney of apoptosis-deficient mice was lower than that in WT mice; n = 5.

(G) PBMCs from female MRL/lpr mice and Bim^{-/-} mice showed reduced levels of apoptotic cells and H₂S. The yellow arrow indicates H₂S, the white indicates apoptotic cells; n = 5; scale bars: 20 μm.

(H and I) STS treatment enhanced the blood H₂S concentration in MRL/lpr mice, whereas Z-VAD treatment decreased H₂S concentration; n = 5.

(J–M) STS treatment increased H₂S concentration in the liver, lung, spleen, and kidney of MRL/lpr mice, which was inhibited by Z-VAD treatment, n = 5.

(N) STS treatment promoted the apoptosis and H₂S generation in PBMCs of MRL/lpr mice, which was alleviated by Z-VAD. The yellow arrow indicated H₂S, the white indicated apoptotic cells; n = 5; scale bars: 20 μm. *p < 0.05; **p < 0.01; ***p < 0.001.

and lipids, which can regulate their recipient organs and tissues.^{19,20} In addition, our previous studies showed that both mesenchymal stem cells (MSCs) and T cells have the capability to generate H₂S.^{13,21} However, it has remained unknown whether EVs can inherit their parent cell's ability to produce H₂S.

In this study, we show that apoptosis is required to maintain endogenous H₂S homeostasis. H₂S restrains the aberrant activation of Th17 cells via sulfhydration of selenoprotein F at the C38 site (Sep15^{C38}).

RESULTS

Apoptotic deficiency results in reduced H₂S levels

Apoptosis-deficient MRL/lpr (B6.MRL-Fas/lpr/J) and Bim^{-/-} (B6.129S1-Bcl2l1tm1.1Ast/J) mice show reduced apoptotic rates in the spleen and peripheral blood mononuclear cells (PBMCs) as assessed by terminal deoxynucleotidyl trans-

ferase dUTP nick end labeling (TUNEL) staining and flow cytometry analysis, respectively (Figures S1A and S1B). Although MRL/lpr and Bim^{-/-} mice have been widely used as SLE disease models,^{22,23} the detailed mechanistic link between apoptotic deficiency and SLE phenotype is not fully elucidated. H₂S, an important gasotransmitter, has emerged as an endogenous regulator of immune homeostasis,¹⁰ but it is unknown whether apoptotic deficiency results in altered H₂S levels.

Therefore, we examined H₂S levels in MRL/lpr and Bim^{-/-} mice and found that the levels of H₂S in the blood were significantly reduced when compared with the wild-type (WT) group as assessed by microelectrode and lead acetate paper assays (Figures 1A and 1B). MRL/lpr and Bim^{-/-} mice also showed significantly reduced levels of H₂S in the liver, lung, spleen, and kidney, but not in the brain, heart, or muscle, when compared with WT mice (Figures 1C–1F and S1C). In addition,

PBMCs from MRL/lpr and Bim^{-/-} mice showed reduced apoptotic rates and lower levels of H₂S compared with WT mice (Figure 1G). These data demonstrate that the levels of H₂S in apoptosis-deficient MRL/lpr and Bim^{-/-} mice are significantly reduced.

Next, we assessed whether apoptotic induction could elevate the levels of H₂S in MRL/lpr mice. Staurosporine (STS) was used to induce *in vivo* apoptosis in MRL/lpr mice, whereas Z-VAD(OMe)-FMK (Z-VAD, a pan-caspase inhibitor) was used to inhibit STS-induced apoptosis.¹ Results showed that STS treatment increased the apoptotic rate of the spleen tissue and PBMCs in MRL/lpr mice, whereas Z-VAD decreased the STS-induced apoptotic rate, confirming the effectiveness of STS-induced apoptosis (Figures S1D and S1E). In MRL/lpr mice, STS treatment enhanced H₂S levels in the blood, liver, lung, spleen, and kidney, which was inhibited by the addition of Z-VAD (Figures 1H–1M). STS also enhanced the apoptotic rate and H₂S generation in PBMCs from MRL/lpr mice, which was also inhibited by the Z-VAD treatment (Figure 1N). These data indicate that *in vivo* apoptotic induction can rescue decreased H₂S levels in MRL/lpr mice.

Apoptotic cells are capable of generating H₂S

Since apoptotic induction can enhance the levels of H₂S in MRL/lpr mice, we examined whether apoptotic cells could generate H₂S. STS and ultraviolet (UV) irradiation were used to induce apoptosis of mouse bone-marrow stem cells (mBMSCs), PBMCs, and CD4⁺ T cells. Z-VAD was used to suppress the apoptosis process (Figures S2A and S2B). Microelectrode assay demonstrated that STS- and UV-induced apoptotic cells showed elevated levels of H₂S in cell supernatant (Figures 2A and 2B). Lead acetate paper assays proved that STS- and UV-induced apoptosis could elevate H₂S levels in the cell supernatant (Figures 2C and 2D). However, pretreatment with Z-VAD decreased the levels of H₂S in the apoptotic cell supernatant (Figures 2A–2D).

In order to further analyze the H₂S production in apoptotic cells, we used STS-induced apoptotic mBMSCs as a model and defined 3, 6, and 9 h after STS treatment as the early, middle, and late stages of apoptosis, respectively (Figures S2C and S2D).²⁴ H₂S microelectrode and H₂S probe staining showed that STS treatment generated H₂S at the early and middle stages of apoptosis compared with control cells (Figures 2E and 2F). During the apoptosis process, there was a significantly elevated expression of CBS, along with a slightly elevated expression of CSE and 3-MST (Figures 2G and 2H). To evaluate the sulphydration levels of mBMSCs at different time points, we used Alexa Fluor 488-conjugated C5 maleimide, which interacts selectively with sulfhydryl groups of cysteines, labeling both sulphydrated and unsulphydrated cysteines (Figure S2E). Dithiothreitol (DTT) was used to selectively cleave disulfide bonds and detach the green signal only from sulphydrated protein, resulting in decreased fluorescence (Figure S2E). Sulphydration levels of mBMSCs were increased at the early and middle stages of apoptosis (Figure 2I). These results indicate that apoptotic mBMSCs generate H₂S mostly at the early and middle stages of apoptosis. Besides, there was no increased fluorescence signaling in the -DTT at 3 or 6 h compared with 0 h. Previous studies showed that sulfhydryl (-SH) groups of cysteines are susceptible to the oxidative modification

caused by increased concentrations of reactive oxygen species (ROS) during apoptosis, resulting in the decrease of -SH contents.^{25,26} Therefore, the decrease of -SH contents during apoptotic process may account for the decrease of fluorescence in the -DTT group at 3 or 6 h.

H₂S deficient mice show an SLE-like phenotype

H₂S plays a vital role in the maintenance of immune homeostasis and H₂S-deficient CBS^{-/-} and CSE^{-/-} mice show significantly impaired immune response.¹⁰ Here, we showed that both CBS^{-/-} and CSE^{-/-} mice display SLE-like disorders such as enlargement of the spleen and lymph nodes (Figure 3A); elevation of serum anti-nuclear antibody (ANA), blood urea nitrogen (BUN), and double-stranded DNA (dsDNA) levels (Figure 3B); impairment of kidney function (Figures 3C and 3D); and immunoglobulin G (IgG) deposition in the spleen and skin (Figure 3E). In addition, Th17 and Th1 cell ratios were higher in the spleen of CBS^{-/-} and CSE^{-/-} mice than that in WT mice, whereas the Treg and Th2 cell ratios were decreased compared with WT mice (Figure 3F). These data suggest that H₂S deficiency may cause an SLE-like disorder.

Apoptosis induction ameliorates SLE phenotypes via elevating the levels of H₂S in MRL/lpr mice

STS treatment alleviated the enlargement of spleen and lymph nodes, decreased the concentration of serum ANA, BUN, and dsDNA, ameliorated kidney damage, and reduced IgG deposition in the kidney and skin of MRL/lpr mice (Figures 4A–4D, S3A, and S3B). These results suggest that STS treatment can alleviate SLE phenotype in MRL/lpr mice. In order to evaluate whether H₂S production contributes to apoptosis-induced therapy for MRL/lpr mice, hydroxylamine hydrochloride (HA), an H₂S-synthesis inhibitor, and propargylglycine (PAG), a CSE inhibitor, were used to block H₂S production.^{27,28} We showed that pretreatment with HA or PAG abolished STS-induced elevation of H₂S in the blood, liver, lung, spleen, and kidney of MRL/lpr mice (Figures S3C–S3H). The addition of HA or PAG increased the weight of spleen and lymph nodes; enhanced concentrations of serum ANA, BUN, and dsDNA; exacerbated kidney damage; and accelerated the IgG deposition in kidney and skin (Figures 4A–4D, S3A, and S3B). Thus, the apoptosis-induced therapy for SLE mice was abolished by the addition of H₂S inhibitors. These data indicate that H₂S plays a pivotal role in apoptosis-induced therapy in SLE mice.

Apoptotic-cell-generated H₂S inhibits aberrant Th17 cell differentiation in MRL/lpr mice

T cell isotype disorder may contribute to the pathogenesis of SLE.²⁹ Therefore, we evaluated the effects of apoptosis-induced therapy on T cell isotype distribution in the spleen of MRL/lpr mice. STS treatment reduced the level of CD4⁺IL-17⁺ Th17 cells and slightly promoted the level of CD4⁺Foxp3⁺ Treg and CD4⁺IL-4⁺ Th2 cells in the spleen of MRL/lpr mice (Figures 4E–4H). However, HA or PAG treatment blocked the inhibitory effect of STS induction for Th17 cells (Figure 4E). These data suggest that apoptosis-induced therapy can inhibit aberrant Th17 cell differentiation in MRL/lpr mice while inhibiting the H₂S production impairs the inhibitory function of apoptosis-induced therapy for Th17 cell differentiation.

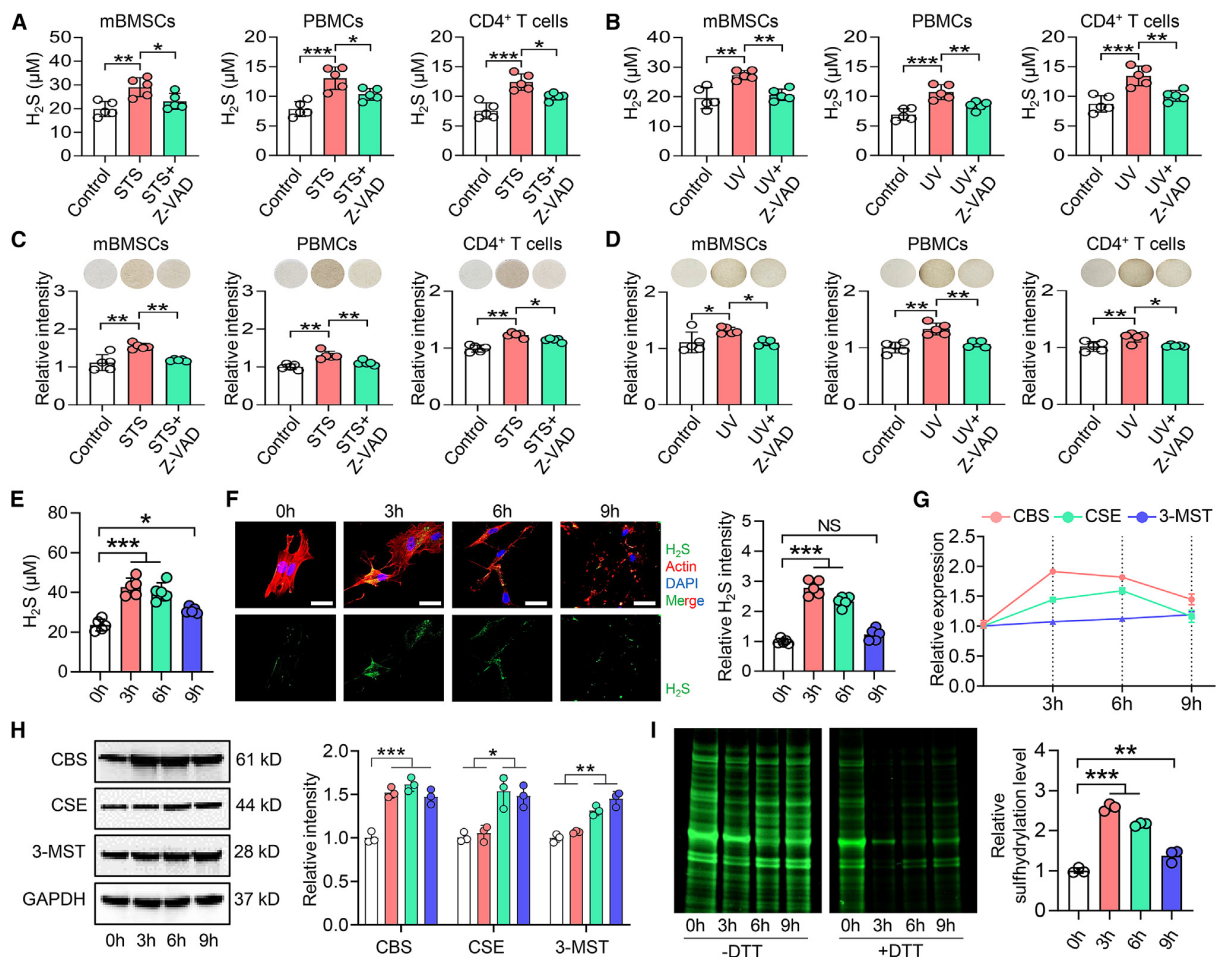


Figure 2. Apoptotic cells release H₂S in vitro

(A–D) After apoptotic induction (STS and UV treatment), the H₂S concentration from the supernatants of different cells was assessed using H₂S microelectrode (A and B) and lead acetate formation test (C and D); n = 5 per group. Both H₂S microelectrode results and lead acetate formation test demonstrated that STS and UV treatment significantly increased the H₂S concentration in mBMSCs, PBMCs, and CD4⁺ T cells, whereas the H₂S concentration was reduced by the addition of Z-VAD (a pan-caspase inhibitor).

(E) H₂S concentration at different time points during STS stimulation was examined by H₂S microelectrode. The H₂S concentrations at 3 and 6 h were higher than control cells; n = 5.

(F) STS induced obvious H₂S generation at 3 and 6 h, whereas H₂S generation decreased at 9 h postinduction; scale bars: 20 μm.

(G) The expression of H₂S-generating enzymes was assessed by quantitative reverse-transcription PCR (RT-qPCR). STS treatment obviously promoted the gene expression of CBS and CSE at 3 and 6 h of STS treatment; n = 3.

(H and I) (H) CBS expression increased at 3, 6, and 9 h of STS treatment. CSE and 3-MST expression increased at 6 and 9 h of STS treatment, n = 3. (I) Green maleimide assay was used to detect sulfhydrylation in mBMSCs lysates after STS induction. STS treatment could enhance the sulfhydrylation of mBMSCs at 3 and 6 h post-STS treatment; n = 3. NS, not significant. *p < 0.05; **p < 0.01; ***p < 0.001.

Next, we evaluated the effects of H₂S on Th17 cell differentiation. Flow cytometry analysis showed that treatment with the H₂S donor NaHS directly inhibited Th17 cell differentiation *in vitro*, whereas HA treatment promoted Th17 cell differentiation (Figure 5A). Both treatments showed a dose-dependent effect. Neither NaHS nor HA treatment affected Th17 cell proliferation or viability (Figures S4A and S4B). The expression levels of Th17 cell differentiation genes including *interleukin-17 (IL-17)*, *retinoic acid orphan receptor gamma T (RORγT)*, *IL-23R*, and *chemokine receptor 6 (CCR6)* were inhibited by NaHS treatment,

but promoted by HA treatment (Figure 5B). In MRL/lpr mice, NaHS treatment reduced the levels of Th17 cells in the spleen and blood, whereas HA treatment enhanced the differentiation of Th17 cells (Figures S4C and S4D). These data reveal that H₂S inhibits Th17 cell differentiation both *in vitro* and *in vivo*.

H₂S regulates Th17 cell differentiation via sulfhydrylation of Sep15

H₂S exerts biological function and molecular regulation predominantly via protein sulfhydrylation (SHY).³⁰ SHY, a type of

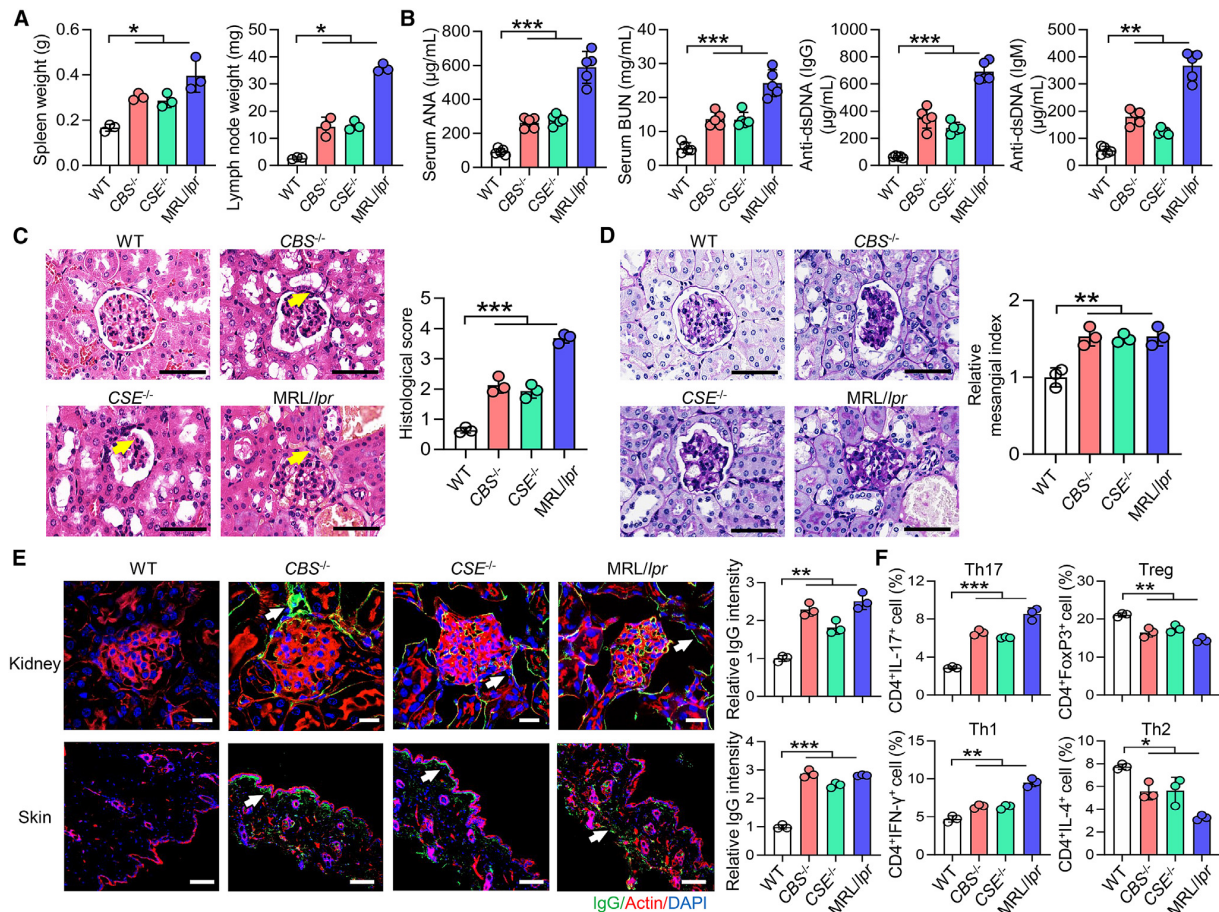


Figure 3. H₂S deficient mice show SLE-like phenotypes

(A) The spleen and lymph nodes weight in female CBS^{-/-}, CSE^{-/-}, and MRL/lpr mice were increased compared with WT mice; n = 3 per group. (B) The concentration of serum ANA, BUN, and dsDNA (IgG and IgM) in CBS^{-/-}, CSE^{-/-}, and MRL/lpr mice were higher than WT mice; n = 5. (C and D) H&E and PAS staining results showed the kidney damage in CBS^{-/-}, CSE^{-/-}, and MRL/lpr mice; the arrow indicates that the glomerular margin is broken (C); n = 3; scale bars: 200 μm. (E) Confocal assay confirmed IgG deposition in the kidney and skin of CBS^{-/-}, CSE^{-/-}, and MRL/lpr mice, the arrow indicates the IgG deposition; n = 3; scale bars: 20 μm for kidney, 100 μm for skin. (F) Flow cytometry showed that the ratio of CD4⁺IL-17⁺ Th17 cells and CD4⁺IFN-γ⁺ Th1 cells increased in the spleen of CBS^{-/-}, CSE^{-/-}, and MRL/lpr mice, whereas the ratio of CD4⁺Foxp3⁺ Treg cells and CD4⁺IL-4⁺ Th2 cells decreased compared with WT mice; n = 3; *p < 0.05; **p < 0.01; ***p < 0.001.

post-translational modification, is a physiological process in which H₂S adds an additional sulfur to the thiol (-SH) group of a cysteine, yielding a hydropersulfide (-SSH).³¹ To explore the mechanism by which H₂S regulates Th17 cell differentiation, we performed quantitative proteomics and specifically H₂S-mediated sulfhydrylation modification proteomics of low-pH quantitative thiol reactivity profiling (low-pH QTRP) (Figures 5C, 5D, and S4E).³² Proteomics showed that 444 proteins were upregulated, 364 proteins were downregulated, and 2641 proteins were unchanged in NaHS-treated Th17 cells compared with the control (Figure 5C; Table S1). In addition, we obtained 145 sulfhydrylation protein targets significantly increased in NaHS-treated Th17 cells group by low-pH QTRP (Table S2). Based on the unchanged protein in proteomics, low-pH QTRP, and Th17 cell differentiation-related

pathways, we selected the top 3 of 10 protein targets for further analysis: Sep15, pyruvate kinase (PKM), and nuclear factor NF-κB p105 subunit (Nfkb1) (Figure 5D). According to the cysteine residues, we generated sulfhydrylation site mutant constructs tagged with FLAG (Sep15^{C38A}, PKM^{C49A}, Nfkb1^{C159A}) (Figures 5E, 5F, and S4F–S4H) and then evaluated the inhibitory effects of H₂S treatment on Th17 cell differentiation. *In vitro* differentiation results showed that Sep15^{C38A}, but not PKM^{C49A} or Nfkb1^{C159A}, impaired the inhibitory effect of H₂S on Th17 cell differentiation after treatment with H₂S (Figures 5G and S4I). In addition, the mutant of Sep15^{C38A} also impaired the inhibitory function of H₂S on the expression of Th17 cell differentiation-related genes (Figure 5H). These data indicate that Sep15 is a potential target for the inhibitory effect of H₂S on Th17 cell differentiation. Next, we evaluated

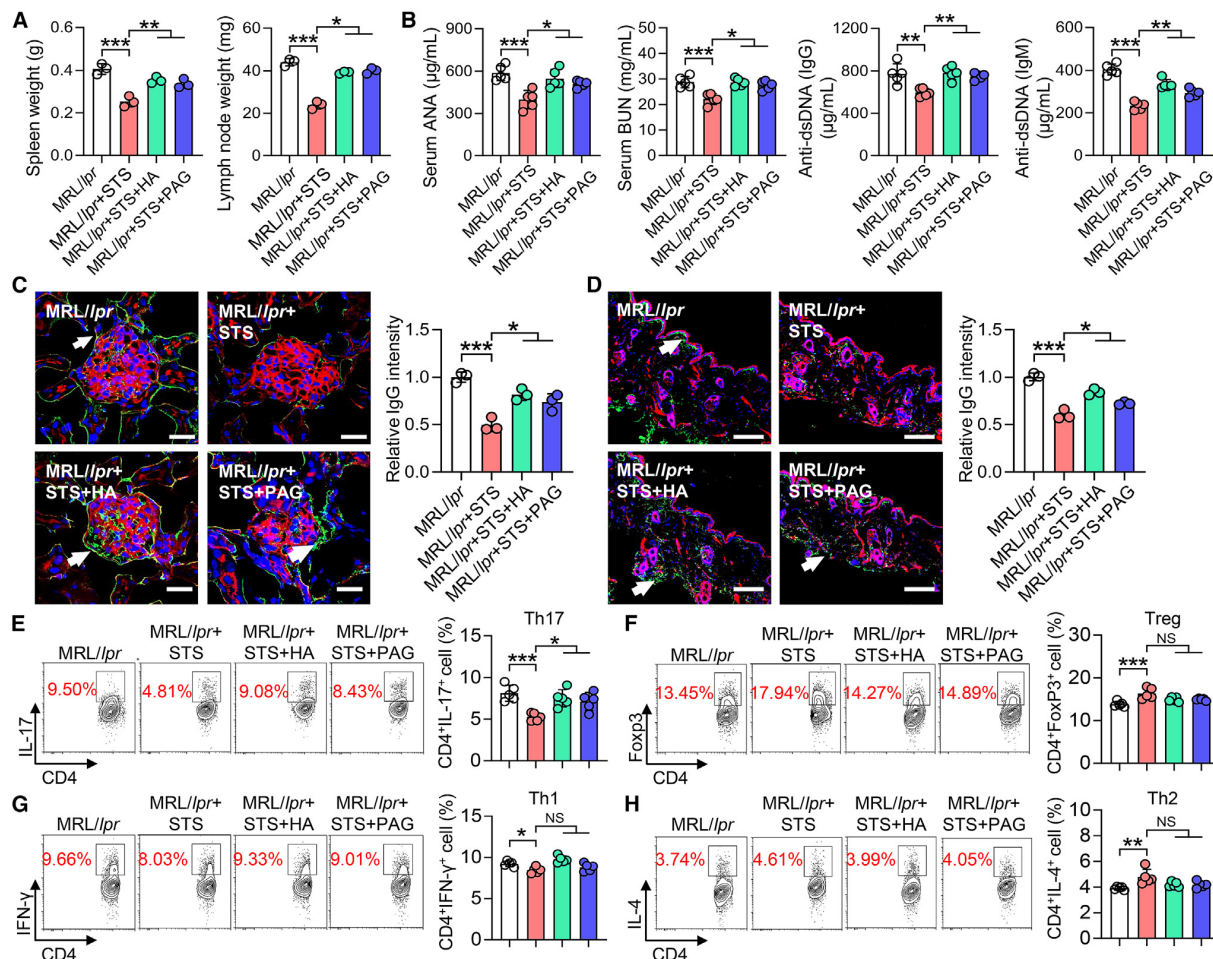


Figure 4. Apoptotic induction alleviates SLE phenotype via elevation of H₂S

(A–D) STS alleviated the enlargement of spleen and lymph nodes (A) (n = 3 per group); decreased the concentration of serum ANA, BUN, and dsDNA (B) (n = 5); and mitigated the IgG deposition in the spleen and skin (C and D, respectively); the arrow indicates the IgG deposition; n = 3; scale bars: 20 µm for kidney, 100 µm for skin), but the effects of STS on female MRL/lpr mice were inhibited by HA or PAG pretreatment.

(E–H) Representative flow cytometric plots and the frequencies of CD4⁺IL-17⁺ Th17 cells, CD4⁺Foxp3⁺ Treg cells, CD4⁺IFN-γ⁺ Th1 cells, and CD4⁺IL-4⁺ Th2 cells, respectively, from the spleens of MRL/lpr mice. STS treatment significantly inhibited the levels of Th17 cells, which was rescued by HA or PAG pretreatment. n = 5; NS, not significant; *p < 0.05, **p < 0.01, ***p < 0.001.

the ratio of Th17 cells in Sep15^{-/-} mice and found that the CD4⁺IL-17⁺ Th17 cell ratio was increased in the spleen and blood of Sep15^{-/-} mice (Figures S5A and S5B). These results suggest that Sep15 plays an important role in inhibiting Th17 cell differentiation.

To confirm the sulfhydrylation modification of Sep15, we used Alexa Fluor 488-conjugated C5 maleimide (Figure S5C). Th17 cells from WT mice showed green bands representing proteins with -SH and -SSH groups in the presence of L-cysteine. DTT treatment reduced the green Sep15 signal in the presence of L-cysteine in Th17 cells from WT mice, indicating sulfhydrylation modification of Sep15 (Figure 5). By contrast, DTT treatment failed to reduce the green signal of Sep15 in CBS^{-/-} Th17 cells, indicating that CBS-generated H₂S is required to maintain Sep15 sulfhydrylation (Figure 5). However, NaHS treatment restored the

sulfhydrylation of Sep15 in CBS^{-/-} Th17 cells (Figure 5J), suggesting that Sep15 can be directly sulfhydrylated by H₂S. In addition, the expression level of Sep15 was not significantly altered in NaHS-treated or CBS^{-/-} mice (Figure S5D). These results indicate that H₂S inhibits Th17 aberrant differentiation via sulfhydrylation of Sep15^{C38A}.

H₂S inhibits Th17 cell differentiation via the Sep15/STAT1/STAT3 axis

The STAT family is essential for Th17 cell differentiation, and in particular, signal transducer and activator of transcription 1 (STAT1) and STAT3 have antagonistic effects on Th17 cell differentiation.³³ STAT1 inhibits Th17 cell differentiation, whereas STAT3 promotes it.⁵ STAT1 can heterodimerize with STAT3 and inhibit STAT3-dependent transcription.^{5,34} We found that

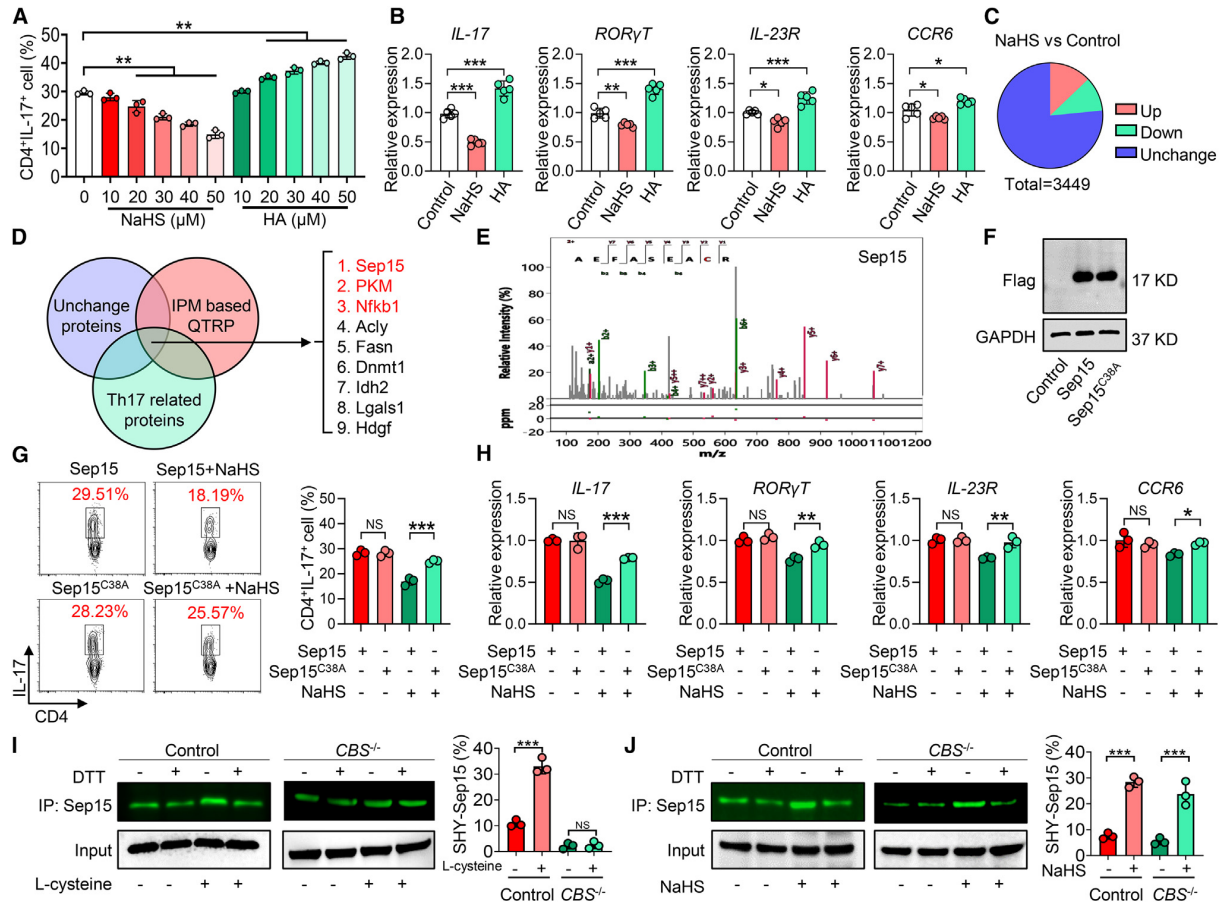


Figure 5. Sulphydration of Sep15 is essential for the inhibitory effect of H₂S on Th17 cell differentiation

(A) Flow cytometry analyzed Th17 cell differentiation ratios under NaHS and HA treatment. NaHS (20, 30, 40, and 50 μ M) inhibited Th17 cell differentiation, whereas HA (20, 30, 40, and 50 μ M) promoted Th17 cell differentiation in a dose-dependent manner; $n = 3$ per group.

(B) Th17-related gene expression was assessed by RT-qPCR. NaHS (50 μ M) treatment inhibited the expression of *IL-17*, *ROR γ T*, *IL-23R*, and *CCR6*, whereas HA (50 μ M) treatment increased their expression; $n = 5$.

(C) Proteomics showed that 444 proteins were upregulated, 364 proteins were downregulated, and 2,641 proteins were unchanged in NaHS-treated Th17 cells compared with the control.

(D) The strategy of combining the unchanged protein in proteomics, low-pH QTRP, and Th17-related proteins was used to analyze potential targets, and 9 potential targets were shown.

(E) C38 of Sep15 is a target site of sulphydration in Th17 cells—fully annotated higher energy collisional dissociation mass spectrometry/mass spectrometry (HCD MS/MS) spectra of the light and heavy 2-iodo-N-(prop-2-yn-1-yl) acetamide (IPM)-modified disulfide peptides.

(F) The construct of Sep15^{C38A} mutant tagged with FLAG was assessed by western blotting.

(G) Th17 cell differentiation was analyzed by flow cytometry. H₂S inhibited Th17 cell differentiation *in vitro*, whereas the Sep15^{C38A} mutant abolished the inhibitory effect of H₂S; $n = 3$.

(H) H₂S inhibited the Th17 cell differentiation-related gene expression, which was impaired in the Sep15^{C38A} cells; $n = 3$.

(I and J) Protein sulphydration in Th17 cells, with or without NaHS treatment, was assessed by Alexa Fluor 488-conjugated C5 maleimide. The green signal of Sep15 protein after L-cysteine treatment (I) or NaHS treatment (J) of Th17 cells from the spleen of WT or CBS^{-/-} mice confirm that Sep15 could be modified by sulphydration under H₂S treatment. $n = 3$; NS, not significant; * $p < 0.05$; ** $p < 0.01$; *** $p < 0.001$.

STAT1 phosphorylation and nuclear translocation were decreased during Th17 cell differentiation (Figures 6A–6C), whereas STAT3 showed the opposite effect, with the augmentation of STAT3 phosphorylation and nuclear translocation (Figures 6A and 6B). Immunoprecipitation-mass spectrometry (IP-MS) and coIP assay confirmed that Sep15 could bind with STAT1, but not with STAT3, STAT4, or STAT5 (Figures 6D and

S6A), suggesting that Sep15 might exert its function through STAT1. In addition, H₂S increased the interaction of Sep15 with STAT1, whereas H₂S failed to promote the interaction between Sep15^{C38A} and STAT1 (Figures 6E, 6F, and S6B). In the STAT family, phosphorylation is the essential prerequisite for nuclear localization and subsequent biological activity.³³ Interestingly, we found that H₂S could promote STAT1 phosphorylation

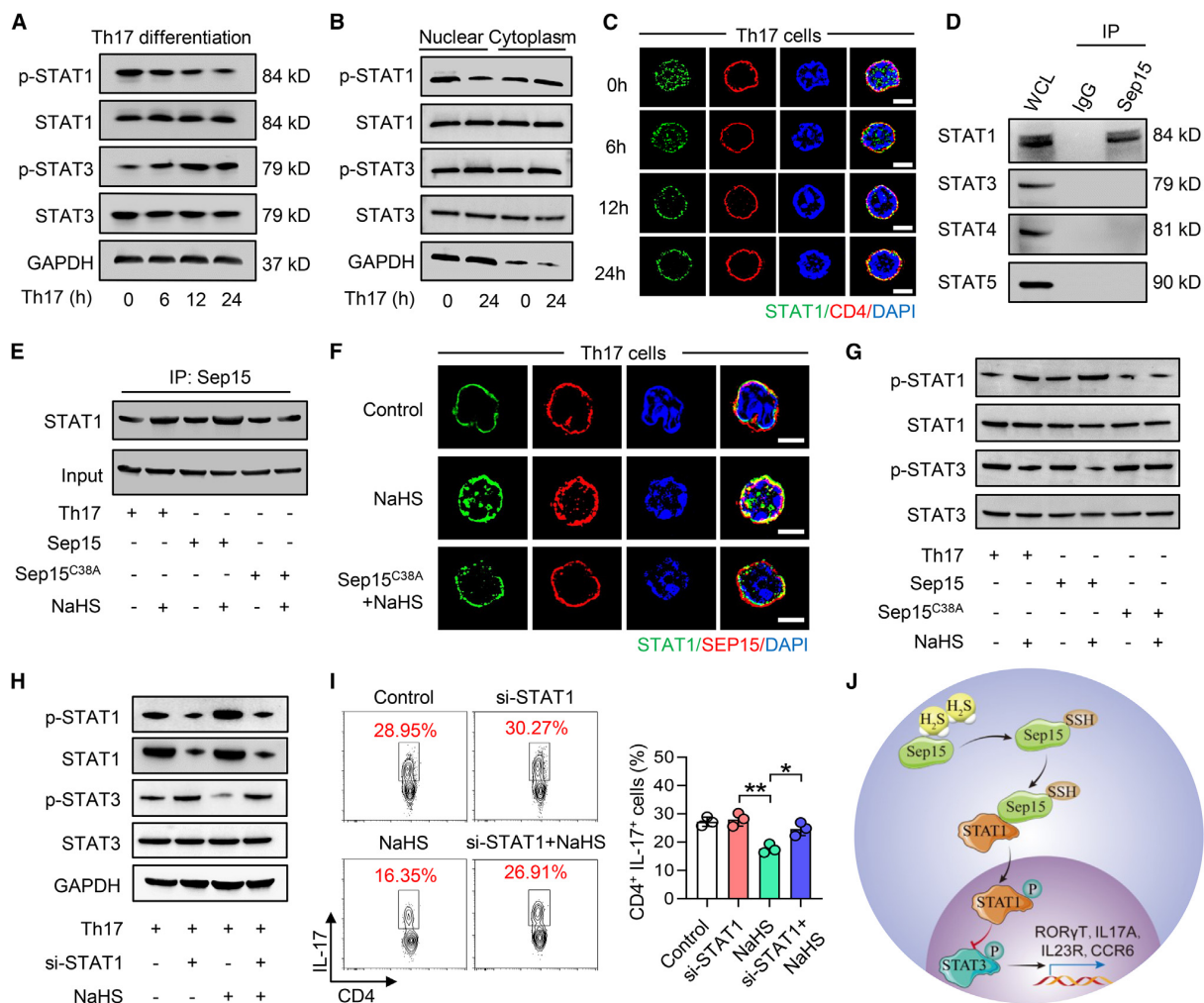


Figure 6. H₂S inhibits Th17 cell differentiation through the Sep15/STAT1/STAT3 signaling axis

(A) The expression of p-STAT1 and p-STAT3 in CD4⁺ T cells during Th17 cell differentiation was evaluated by western blotting. The expression of p-STAT1 decreased during Th17 cell differentiation, whereas p-STAT3 expression increased.
 (B) During Th17 cell differentiation, nuclear p-STAT1 expression decreased, whereas nuclear p-STAT3 expression increased.
 (C) STAT1 staining showed that the amount of nuclear p-STAT1 reduced at 24 h after Th17 stimulation; scale bars: 5 μm.
 (D) CoIP showed that Sep15 interacted with STAT1.
 (E) H₂S promoted the interaction between Sep15 and STAT1, whereas Sep15^{C38A} mutation impaired this interaction.
 (F) H₂S failed to promote the nuclear STAT1 expression and the interaction between STAT1 and Sep15 in the Sep15^{C38A} mutant Th17 cells; scale bars; 5 μm.
 (G) H₂S promoted the p-STAT1 expression and inhibited the p-STAT3 expression in Th17 cells, but these effects were not observed in Sep15C38A mutants.
 (H) H₂S failed to inhibit p-STAT3 expression in Th17 cells when STAT1 was knocked down by siRNA.
 (I) The knockdown of STAT1 impaired the inhibitory effect of H₂S on the Th17 cells; n = 3.
 (J) The schematic graph of Sep15/STAT1/STAT3 axis in the inhibitory effect of H₂S on Th17 cell differentiation. *p < 0.05, **p < 0.01.

and inhibit STAT3 phosphorylation, but these effects were impaired when Sep15^{C38} sulfhydryl site was mutated to Sep15^{C38A} (Figures 6G and S6C–S6E). These results indicate that H₂S sulfhydrates Sep15 at the C38 site and promotes the interaction between Sep15 and STAT1, which facilitates the phosphorylation and nuclear localization of STAT1.

Next, we further validated the function of STAT1 in the differentiation of Th17 cells by knocking down STAT1 expression

with small interfering RNA (siRNA) (Figure S6F). The result showed that H₂S inhibited the phosphorylation of STAT3, but the effect was suppressed by the knockdown of STAT1 (Figure 6H). The inhibitory effect of H₂S on Th17 cell differentiation and related gene expression was also impaired when STAT1 expression was knocked down (Figures 6I and S6G), suggesting that the inhibitory effect of H₂S is associated with the Sep15/STAT1/STAT3 axis (Figure 6J).

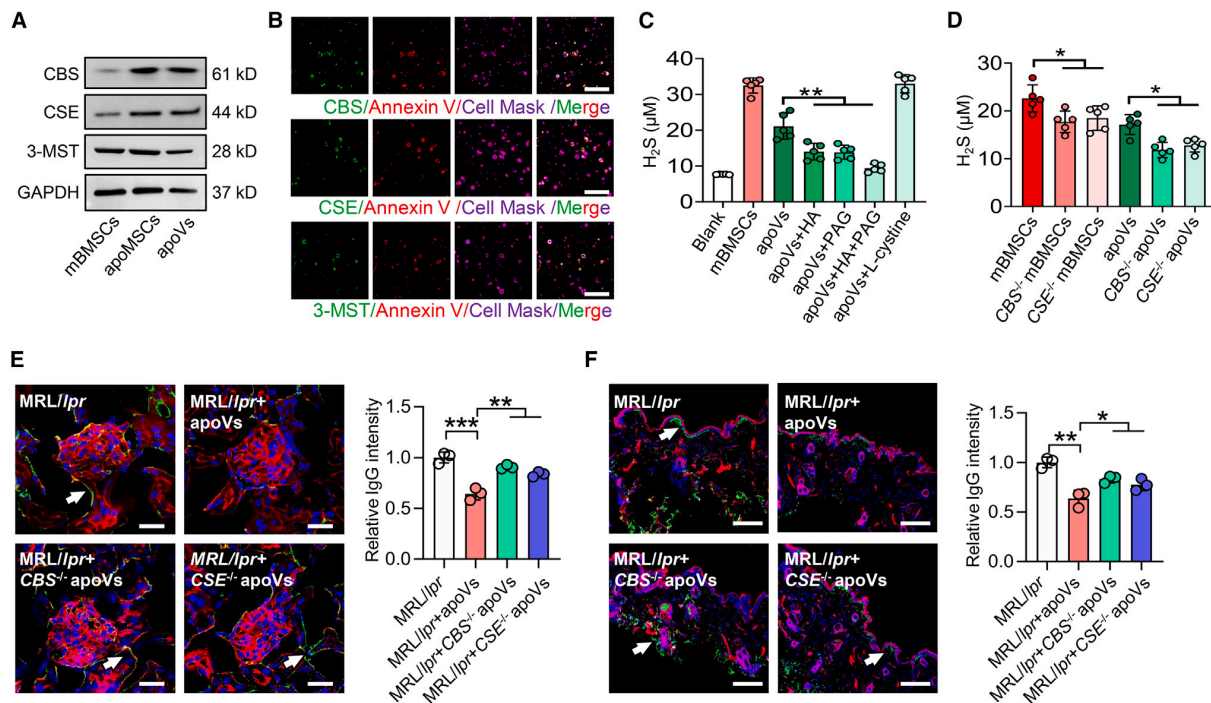


Figure 7. H₂S is required for apoV-mediated SLE therapy

(A) The expressions of CBS, CSE, and 3-MST in mBMSCs, apoptotic mBMSCs (apoMSCs), and apoVs were assessed by western blotting. (B) The expressions of CBS, CSE, and 3-MST in apoVs were evaluated by immunofluorescence; scale bars: 1 μ m. (C) H₂S microelectrode showed that apoVs generated H₂S, which was inhibited by HA and PAG treatment; n = 5 per group. (D) The H₂S concentration from CBS^{-/-} and CSE^{-/-} apoVs was lower than that in apoVs; n = 5. (E and F) ApoVs suppressed IgG deposition in the spleen and skin; the arrow indicates the IgG deposition. n = 3; scale bars: 20 μ m for kidney, 100 μ m for skin, whereas the function was impaired in CBS^{-/-} apoVs and CSE^{-/-} apoVs. *p < 0.05; **p < 0.01; ***p < 0.001

ApoVs generate H₂S

ApoVs are metabolic products of the apoptotic cells that possess multiple biological functions.³⁵ Our previous study showed that MSCs express the key H₂S-generating enzymes CBS and CSE and have the capability of generating H₂S.²¹ Here, we found that apoptotic mBMSCs (apoMSCs) and apoVs expressed CBS, CSE, and 3-MST (Figures 7A, 7B, and S7A). Microelectrode assay showed that apoVs could generate H₂S, whereas HA or PAG treatment inhibited the H₂S concentration generated by apoVs (Figure 7C). In addition, we collected apoVs from CBS^{-/-} mBMSCs and CSE^{-/-} mBMSCs, named CBS^{-/-} apoVs and CSE^{-/-} apoVs, respectively (Figure S7B). Microelectrode assay showed the H₂S concentration from CBS^{-/-} apoVs and CSE^{-/-} apoVs was lower than apoVs (Figure 7D). In addition, siRNA was used to knock down 3-MST levels in mBMSCs and the si-3-MST apoVs were collected from cells (Figure S7C). Results showed that the H₂S level in si-3-MST apoVs was lower than that in apoVs (Figure S7D). Therefore, these studies demonstrate that apoVs have the ability to generate H₂S.

Our previous study showed that apoVs can ameliorate SLE and arthritis phenotypes.³⁶ In order to further explore the relationship between H₂S generation and the therapeutical efficacy of apoVs for SLE mice, apoVs were collected and systemically infused into MRL/lpr mice. Results showed that apoVs alleviated SLE phenotypes in MRL/lpr mice, as evidenced by reducing the

weight of the spleen and lymph nodes (Figure S7E); decreasing the levels of serum ANA, BUN, and dsDNA (Figure S7F); relieving kidney damage; and inhibiting IgG deposition in the kidney and skin (Figures 7E, 7F, S7G, and S7H). However, both CBS^{-/-} apoVs and CSE^{-/-} apoVs failed to exert such therapeutic effects in MRL/lpr mice (Figures 7E, 7F, and S7E–S7H). These data suggest that apoVs can generate H₂S, which is required for the therapeutic effect in SLE mice.

DISCUSSION

Apoptosis is an essential process to maintain organ and tissue homeostasis.^{3,6} Apoptotic cells and vesicles are not waste; rather, they release necessary products and signals to actively modulate the recipient microenvironment and neighboring cells.¹ In this study, we identified that apoptotic cells are capable of generating H₂S, suggesting an intrinsic connection between cell apoptosis and H₂S production. In addition, apoVs can generate H₂S with the expression of CBS, CSE, and 3-MST.

Billions of cells undergo apoptosis every day in the human body to generate significant amounts of apoVs.^{19,37} ApoVs, a specific type of EVs, contain a variety of DNAs, RNAs, proteins, lipids, and nuclear components.³⁸ We identified that apoVs express specific markers such as Fas, calnexin, and calreticulin when compared with exosomes.³⁹ In addition, our previous

study showed that apoVs are required to maintain mesenchymal stem cell homeostasis and rescue osteoporosis phenotype via transferring miRNA.¹⁹ ApoVs are capable of promoting wound healing and hair regeneration via activation of Wnt/ β -catenin pathway in skin and hair follicle MSCs.⁴⁰ Small EVs inherit the glutathione-related protein (GSTM2) to ameliorate senescence and aging by increasing the antioxidant capacity in old mice.⁴¹ A previous study showed that pretreating MSCs with H₂S could enhance the therapeutic effect of MSC-EVs on hypoxic-ischemic injury, suggesting that H₂S is important for the formation and/or function of EVs.⁴² Here, we show that apoVs inherit the H₂S-generating ability from their parent cells, which is closely associated with apoV-mediated therapeutic effect in SLE mice.

H₂S homeostasis is important for maintenance of the physiological functions of multiple organs, and endogenous H₂S levels are associated with many biological activities, such as exercise and dietary restriction.^{7,43} Exercise promotes skeletal muscle angiogenesis via elevating endogenous H₂S levels.⁸ Sulfur amino-acid restriction increases endogenous H₂S production to protect the liver from ischemic reperfusion injury.⁷ In this study, we found that apoptosis is a necessary process for maintaining endogenous H₂S homeostasis while generating a relatively large amount of H₂S. Apoptosis defects lead to insufficient levels of H₂S in the blood and multiple organs, thereby affecting immune homeostasis.

H₂S is regarded as a natural buffer for the immune system and it is known that the deficiency of H₂S leads to serious immune disorders.^{44,45} Our previous study indicated that H₂S promotes Treg cell differentiation by sulfhydrating nuclear transcription factor Y subunit beta (NFYB).¹³ Here, we revealed that H₂S can sulfhydrate Sep15, a thioredoxin-like oxidoreductase in the endoplasmic reticulum,⁴⁶ to inhibit Th17 cell differentiation via regulating STAT1 and STAT3. The STAT family plays an important role in T cell proliferation and differentiation. STAT1 has an antagonistic effect on STAT3 during Th17 cell differentiation.⁵ STAT3 phosphorylation promotes the expression of downstream genes *IL-17* and *ROR γ t*.^{5,47} We found that the sulfhydration of Sep15 facilitates its interaction with STAT1 and promotes STAT1 phosphorylation and nuclear translocation. The nuclear STAT1 inhibits STAT3 phosphorylation, leading to the impairment of Th17 cell differentiation. Interestingly, Sep15 knockout (Sep15^{-/-}) mice show SLE-like phenotypes, including splenomegaly and a high concentration of serum IgG,⁴⁸ indicating that Sep15 may be involved in the pathological process of SLE.

This study reveals that apoptosis is required to maintain H₂S homeostasis. In addition, apoVs inherit H₂S generation capacity from their parent cells. These data reveal a previously unknown H₂S production characteristic of apoptotic cells and apoVs.

Limitations of the study

This study showed that apoptosis is required to maintain endogenous H₂S homeostasis, which was mainly conducted in MRL/*lpr* and *Bim*^{-/-} mice. But whether other apoptosis-deficient mice also show decreased H₂S levels remains to be assessed. Moreover, T cell isotype disorder is closely associated with the pathogenesis of SLE, and this study showed that H₂S attenuated SLE via inhibiting the aberrant differentiation of Th17 cells. In addition, other immune cells are also involved in the initiation

and progression of SLE, such as B cells and macrophages. Therefore, whether H₂S can regulate other immune cells of SLE needs to be further investigated. Finally, this study demonstrated that apoVs could inherit their parent cell's ability to produce H₂S. However, the specific mechanism remains unclear. Further experiments are required to evaluate whether the H₂S-generating mechanism in apoVs is different from that in cells.

STAR★METHODS

Detailed methods are provided in the online version of this paper and include the following:

- KEY RESOURCES TABLE
- RESOURCE AVAILABILITY
 - Lead contact
 - Material availability
 - Data and code availability
- EXPERIMENTAL MODEL AND SUBJECT DETAILS
 - Animals
 - Antibodies and reagents
- METHOD DETAILS
 - Apoptosis modulation
 - Injection of H₂S donor and inhibitor
 - Isolation of mBMSCs
 - Isolation of apoVs
 - Immunofluorescence staining of apoVs
 - Th17 cell differentiation
 - Flow cytometry
 - H₂S microelectrode detection method
 - Lead sulfide detection method
 - H₂S probe staining
 - Western blotting
 - Quantitative PCR analysis
 - Sulfhydration assay using maleimide
 - Click chemistry for H₂S-mediated sulfhydration proteomics
 - LC-MS/MS analysis
 - Generation of site mutant construct
 - RNA-Mediated Interference and Plasmid Transfection
 - Histology
- QUANTIFICATION AND STATISTICAL ANALYSIS

SUPPLEMENTAL INFORMATION

Supplemental information can be found online at <https://doi.org/10.1016/j.cmet.2023.11.012>.

ACKNOWLEDGMENTS

This work was supported by grants from the National Key R&D Program of China (2021YFA1100600 to S.S. and 2022YFA1303000 to C.C.), the Pearl River Talent Recruitment Program (2019ZT08Y485, 2019QN01Y138, and 2019JC01Y182), the Guangdong Financial Fund for High-Caliber Hospital Construction (174-2018-XMZC-0001-03-0125 and D-07 to S.S. and D-11 to X.K.), the Chinese Academy of Sciences Strategic Priority Research Program B grants (XDB39000000 to C.C.), and the National Natural Science Foundation of China (82170924 to X.K. and 32371297 to X.Q.).

AUTHOR CONTRIBUTIONS

Conceptualization, Q.O. and S.S.; methodology, Q.O., X.Q., and Z.L.; investigation, Q.O., X.Q., Z.L., L.N., F.L., R.C., T.X., N.Y., and Y.L.; resources, L.F., J.Y., X.M., and X.K.; funding acquisition, X.Q., X.K., C.C., and S.S.; writing – original draft, Q.O. and X.Q.; writing – review & editing, C.C. and S.S.; supervision, C.C. and S.S. All authors approved the final version of the manuscript.

DECLARATION OF INTERESTS

The authors declare no competing interests.

INCLUSION AND DIVERSITY

We support inclusive, diverse, and equitable conduct of research.

Received: June 27, 2023

Revised: October 4, 2023

Accepted: November 27, 2023

Published: December 18, 2023

REFERENCES

- Medina, C.B., Mehrotra, P., Arandjelovic, S., Perry, J.S.A., Guo, Y., Morioka, S., Barron, B., Walk, S.F., Ghesquière, B., Krupnick, A.S., et al. (2020). Metabolites released from apoptotic cells act as tissue messengers. *Nature* **580**, 130–135.
- Singh, B., Maiti, G.P., Zhou, X., Fazel-Najafabadi, M., Bae, S.C., Sun, C., Terao, C., Okada, Y., Heng Chua, K., Kochi, Y., et al. (2021). Lupus susceptibility region containing CDKN1B rs34330 mechanistically influences expression and function of multiple target genes, also linked to proliferation and apoptosis. *Arthritis Rheumatol.* **73**, 2303–2313.
- Tang, D., Kang, R., Berghe, T.V., Vandenabeele, P., and Kroemer, G. (2019). The molecular machinery of regulated cell death. *Cell Res.* **29**, 347–364.
- Cheng, T., Ding, S., Liu, S., Li, X., Tang, X., and Sun, L. (2021). Resolvin d1 improves the Treg/Th17 imbalance in systemic lupus erythematosus through miR-30e-5p. *Front. Immunol.* **12**, 668760.
- Meyer Zu Horste, G., Przybylski, D., Schramm, M.A., Wang, C., Schnell, A., Lee, Y., Sobel, R., Regev, A., and Kuchroo, V.K. (2018). Fas promotes T helper 17 cell differentiation and inhibits T helper 1 cell development by binding and sequestering transcription factor stat1. *Immunity* **48**, 556–569.e7.
- Anderson, C.J., Medina, C.B., Barron, B.J., Karvelyte, L., Aaes, T.L., Lambert, I., Perry, J.S.A., Mehrotra, P., Gonçalves, A., Lemeire, K., et al. (2021). Microbes exploit death-induced nutrient release by gut epithelial cells. *Nature* **596**, 262–267.
- Hine, C., Harputlugil, E., Zhang, Y., Ruckstuhl, C., Lee, B.C., Brace, L., Longchamp, A., Treviño-Villarreal, J.H., Mejia, P., Ozaki, C.K., et al. (2015). Endogenous hydrogen sulfide production is essential for dietary restriction benefits. *Cell* **160**, 132–144.
- Longchamp, A., Mirabella, T., Arduini, A., Macarthur, M.R., Das, A., Treviño-Villarreal, J.H., Hine, C., Ben-Sahra, I., Knudsen, N.H., Brace, L.E., et al. (2018). Amino acid restriction triggers angiogenesis via gcn2/ atf4 regulation of VEGF and H₂S production. *Cell* **173**, 117–129.e14.
- Hine, C., Kim, H.J., Zhu, Y., Harputlugil, E., Longchamp, A., Matos, M.S., Ramadoss, P., Bauerle, K., Brace, L., Asara, J.M., et al. (2017). Hypothalamic-pituitary axis regulates hydrogen sulfide production. *Cell Metab.* **25**, 1320–1333.e5.
- Cirino, G., Szabo, C., and Papapetropoulos, A. (2023). Physiological roles of hydrogen sulfide in mammalian cells, tissues, and organs. *Physiol. Rev.* **103**, 31–276.
- Kolluru, G.K., Shackelford, R.E., Shen, X., Dominic, P., and Kevil, C.G. (2023). Sulfide regulation of cardiovascular function in health and disease. *Nat. Rev. Cardiol.* **20**, 109–125.
- Wang, Y., Yu, R., Wu, L., and Yang, G. (2020). Hydrogen sulfide signaling in regulation of cell behaviors. *Nitric Oxide* **103**, 9–19.
- Yang, R., Qu, C., Zhou, Y., Konkol, J.E., Shi, S., Liu, Y., Chen, C., Liu, S., Liu, D., Chen, Y., et al. (2015). Hydrogen sulfide promotes Tet1- and Tet2-mediated foxp3 demethylation to drive regulatory T cell differentiation and maintain immune homeostasis. *Immunity* **43**, 251–263.
- Koga, T., Sato, T., Furukawa, K., Morimoto, S., Endo, Y., Umeda, M., Sumiyoshi, R., Fukui, S., Kawashiri, S.Y., Iwamoto, N., et al. (2019). Promotion of calcium/calmodulin-dependent protein kinase 4 by GLUT1-dependent glycolysis in systemic lupus erythematosus. *Arthritis Rheumatol.* **71**, 766–772.
- Voss, K., Sewell, A.E., Krystofiak, E.S., Gibson-Corley, K.N., Young, A.C., Basham, J.H., Sugiura, A., Arner, E.N., Beavers, W.N., Kunkle, D.E., et al. (2023). Elevated transferrin receptor impairs T cell metabolism and function in systemic lupus erythematosus. *Sci. Immunol.* **8**, eabq0178.
- Kono, M., Yoshida, N., Maeda, K., Suárez-Fueyo, A., Kyttaaris, V.C., and Tsokos, G.C. (2019). Glutaminase 1 inhibition reduces glycolysis and ameliorates lupus-like disease in MRL/lpr mice and experimental autoimmune encephalomyelitis. *Arthritis Rheumatol.* **71**, 1869–1878.
- Hochrein, S.M., Wu, H., Eckstein, M., Arrigoni, L., Herman, J.S., Schumacher, F., Gerecke, C., Rosenfeldt, M., Grün, D., Kleuser, B., et al. (2022). The glucose transporter GLUT3 controls T helper 17 cell responses through glycolytic-epigenetic reprogramming. *Cell Metab.* **34**, 516–532.e11.
- Caruso, S., and Poon, I.K.H. (2018). Apoptotic cell-derived extracellular vesicles: more than just debris. *Front. Immunol.* **9**, 1486.
- Liu, D., Kou, X., Chen, C., Liu, S., Liu, Y., Yu, W., Yu, T., Yang, R., Wang, R., Zhou, Y., et al. (2018). Circulating apoptotic bodies maintain mesenchymal stem cell homeostasis and ameliorate osteopenia via transferring multiple cellular factors. *Cell Res.* **28**, 918–933.
- Qu, Y., He, Y., Meng, B., Zhang, X., Ding, J., Kou, X., Teng, W., and Shi, S. (2022). Apoptotic vesicles inherit SOX2 from pluripotent stem cells to accelerate wound healing by energizing mesenchymal stem cells. *Acta Biomater.* **149**, 258–272.
- Liu, Y., Yang, R., Liu, X., Zhou, Y., Qu, C., Kikuri, T., Wang, S., Zandi, E., Du, J., Ambudkar, I.S., et al. (2014). Hydrogen sulfide maintains mesenchymal stem cell function and bone homeostasis via regulation of Ca(2+) channel sulfhydration. *Cell Stem Cell* **15**, 66–78.
- Rizzello, C., Cancila, V., Sangaletti, S., Botti, L., Ratti, C., Milani, M., Dugo, M., Bertoni, F., Tripodo, C., Chiodoni, C., et al. (2022). Intracellular osteopontin protects from autoimmunity-driven lymphoma development inhibiting TLR9-MYD88-STAT3 signaling. *Mol. Cancer* **21**, 215.
- Tsai, F., Homan, P.J., Agrawal, H., Misharin, A.V., Abdala-Valencia, H., Haines, G.K., Dominguez, S., Bloomfield, C.L., Saber, R., Chang, A., et al. (2017). Bim suppresses the development of SLE by limiting myeloid inflammatory responses. *J. Exp. Med.* **214**, 3753–3773.
- Goldblatt, Z.E., Cirka, H.A., and Billiar, K.L. (2021). Mechanical regulation of apoptosis in the cardiovascular system. *Ann. Biomed. Eng.* **49**, 75–97.
- Urbonaviciute, V., Meister, S., Fürnrohr, B.G., Frey, B., Gückel, E., Schett, G., Herrmann, M., and Voll, R.E. (2009). Oxidation of the alarmin high-mobility group box 1 protein (HMGB1) during apoptosis. *Autoimmunity* **42**, 305–307.
- Liedhegner, E.A., Steller, K.M., and Mיעאל, J.J. (2011). Levodopa activates apoptosis signaling kinase 1 (ASK1) and promotes apoptosis in a neuronal model: implications for the treatment of Parkinson's disease. *Chem. Res. Toxicol.* **24**, 1644–1652.
- Asimakopoulou, A., Panopoulos, P., Chasapis, C.T., Coletta, C., Zhou, Z., Cirino, G., Giannis, A., Szabo, C., Spyroulias, G.A., and Papapetropoulos, A. (2013). Selectivity of commonly used pharmacological inhibitors for cystathionine beta synthase (CBS) and cystathionine gamma lyase (CSE). *Br. J. Pharmacol.* **169**, 922–932.
- Papapetropoulos, A., Whiteman, M., and Cirino, G. (2015). Pharmacological tools for hydrogen sulphide research: a brief, introductory guide for beginners. *Br. J. Pharmacol.* **172**, 1633–1637.

29. Kim, D.S., Park, Y., Choi, J.W., Park, S.H., Cho, M.L., and Kwok, S.K. (2021). Lactobacillus acidophilus supplementation exerts a synergistic effect on tacrolimus efficacy by modulating Th17/Treg balance in lupus-prone mice via the SIGNR3 pathway. *Front. Immunol.* **12**, 696074.
30. Luo, S., Kong, C., Zhao, S., Tang, X., Wang, Y., Zhou, X., Li, R., Liu, X., Tang, X., Sun, S., et al. (2023). Endothelial hdac1-zeb2-nurd complex drives aortic aneurysm and dissection through regulation of protein S-sulfhydration. *Circulation* **147**, 1382–1403.
31. Zivanovic, J., Kouroussis, E., Kohl, J.B., Adhikari, B., Bursac, B., Schott-Roux, S., Petrovic, D., Mijjkovic, J.L., Thomas-Lopez, D., Jung, Y., et al. (2019). Selective persulfide detection reveals evolutionarily conserved antiaging effects of S-sulfhydration. *Cell Metab.* **30**, 1152–1170.e13.
32. Fu, L., Li, Z., Liu, K., Tian, C., He, J., He, J., He, F., Xu, P., and Yang, J. (2020). A quantitative thiol reactivity profiling platform to analyze redox and electrophile reactive cysteine proteomes. *Nat. Protoc.* **15**, 2891–2919.
33. Stabile, H., Scarno, G., Fionda, C., Gismondi, A., Santoni, A., Gadina, M., and Sciumè, G. (2018). JAK/STAT signaling in regulation of innate lymphoid cells: the gods before the guardians. *Immunol. Rev.* **286**, 148–159.
34. Villarino, A.V., Kanno, Y., and O’Shea, J.J. (2017). Mechanisms and consequences of Jak-STAT signaling in the immune system. *Nat. Immunol.* **18**, 374–384.
35. Zheng, C., Sui, B., Zhang, X., Hu, J., Chen, J., Liu, J., Wu, D., Ye, Q., Xiang, L., Qiu, X., et al. (2021). Apoptotic vesicles restore liver macrophage homeostasis to counteract type 2 diabetes. *J. Extracell. Vesicles* **10**, e12109.
36. Wang, R., Hao, M., Kou, X., Sui, B., Sanmillan, M.L., Zhang, X., Liu, D., Tian, J., Yu, W., Chen, C., et al. (2023). Apoptotic vesicles ameliorate lupus and arthritis via phosphatidylserine-mediated modulation of T cell receptor signaling. *Bioact. Mater.* **25**, 472–484.
37. Phan, T.K., Ozkocak, D.C., and Poon, I.K.H. (2020). Unleashing the therapeutic potential of apoptotic bodies. *Biochem. Soc. Trans.* **48**, 2079–2088.
38. Santavanond, J.P., Rutter, S.F., Atkin-Smith, G.K., and Poon, I.K.H. (2021). Apoptotic bodies: mechanism of formation, isolation and functional relevance. *Subcell. Biochem.* **97**, 61–88.
39. Zhang, X., Tang, J., Kou, X., Huang, W., Zhu, Y., Jiang, Y., Yang, K., Li, C., Hao, M., Qu, Y., et al. (2022). Proteomic analysis of MSC-derived apoptotic vesicles identifies Fas inheritance to ameliorate haemophilia A via activating platelet functions. *J. Extracell. Vesicles* **11**, e12240.
40. Ma, L., Chen, C., Liu, D., Huang, Z., Li, J., Liu, H., Kin Kwok, R.T., Tang, B., Sui, B., Zhang, X., et al. (2023). Apoptotic extracellular vesicles are metabolized regulators nurturing the skin and hair. *Bioact. Mater.* **19**, 626–641.
41. Fafián-Labora, J.A., Rodríguez-Navarro, J.A., and O’Loughlin, A. (2020). Small extracellular vesicles have GST activity and ameliorate senescence-related tissue damage. *Cell Metab.* **32**, 71–86.e5.
42. Chu, X., Liu, D., Li, T., Ke, H., Xin, D., Wang, S., Cao, Y., Xue, H., and Wang, Z. (2020). Hydrogen sulfide-modified extracellular vesicles from mesenchymal stem cells for treatment of hypoxic-ischemic brain injury. *J. Control. Release* **328**, 13–27.
43. Das, A., Huang, G.X., Bonkowski, M.S., Longchamp, A., Li, C., Schultz, M.B., Kim, L.J., Osborne, B., Joshi, S., Lu, Y., et al. (2018). Impairment of an endothelial NAD(+)-H₂S signaling network is a reversible cause of vascular aging. *Cell* **173**, 74–89.e20.
44. Huerta de la Cruz, S., Santiago-Castañeda, C.L., Rodríguez-Palma, E.J., Medina-Terol, G.J., López-Preza, F.I., Rocha, L., Sánchez-López, A., Freeman, K., and Centurión, D. (2022). Targeting hydrogen sulfide and nitric oxide to repair cardiovascular injury after trauma. *Nitric Oxide* **129**, 82–101.
45. Pozzi, G., Gobbi, G., Masselli, E., Carubbi, C., Presta, V., Ambrosini, L., Vitale, M., and Mirandola, P. (2022). Buffering adaptive immunity by hydrogen sulfide. *Cells* **11**, 325.
46. Goltyshev, M.V., Mal’tseva, V.N., and Varlamova, E.G. (2020). Expression of ER-resident selenoproteins and activation of cancer cells apoptosis mechanisms under ER-stress conditions caused by methylseleninic acid. *Gene* **755**, 144884.
47. Masuda, K., Ripley, B., Nyati, K.K., Dubey, P.K., Zaman, M.M., Hanieh, H., Higa, M., Yamashita, K., Standley, D.M., Mashima, T., et al. (2016). Arid5a regulates naive CD4+ T cell fate through selective stabilization of Stat3 mRNA. *J. Exp. Med.* **213**, 605–619.
48. Yim, S.H., Everley, R.A., Schildberg, F.A., Lee, S.G., Orsi, A., Barbati, Z.R., Karatepe, K., Fomenko, D.E., Tsuji, P.A., Luo, H.R., et al. (2018). Role of selenof as a gatekeeper of secreted disulfide-rich glycoproteins. *Cell Rep.* **23**, 1387–1398.
49. Misu, N., Zhang, M., Mori, S., Miyazaki, T., Furukawa, H., Sasaki, T., Nose, M., and Ono, M. (2007). Autosomal loci associated with a sex-related difference in the development of autoimmune phenotypes in a lupus model. *Eur. J. Immunol.* **37**, 2787–2796.
50. Eipel, C., Bordel, R., Nickels, R.M., Menger, M.D., and Vollmar, B. (2004). Impact of leukocytes and platelets in mediating hepatocyte apoptosis in a rat model of systemic endotoxemia. *Am. J. Physiol. Gastrointest. Liver Physiol.* **286**, G769–G776.
51. Ou, Q., Tan, L., Shao, Y., Lei, F., Huang, W., Yang, N., Qu, Y., Cao, Z., Niu, L., Liu, Y., et al. (2022). Electrostatic charge-mediated apoptotic vesicle biodistribution attenuates sepsis by switching neutrophil netosis to apoptosis. *Small* **18**, e2200306.
52. Hanna, J., Beke, F., O’Brien, L.M., Kapeni, C., Chen, H.C., Carbonaro, V., Kim, A.B., Kishore, K., Adolph, T.E., Skjoed, M.O., et al. (2022). Cell-autonomous hedgehog signaling controls th17 polarization and pathogenicity. *Nat. Commun.* **13**, 4075.
53. Bithi, N., Link, C., Henderson, Y.O., Kim, S., Yang, J., Li, L., Wang, R., Willard, B., and Hine, C. (2021). Dietary restriction transforms the mammalian protein persulfidome in a tissue-specific and cystathionine gamma-lyase-dependent manner. *Nat. Commun.* **12**, 1745.
54. Peng, B., Chen, W., Liu, C., Rosser, E.W., Pacheco, A., Zhao, Y., Aguilar, H.C., and Xian, M. (2014). Fluorescent probes based on nucleophilic substitution-cyclization for hydrogen sulfide detection and bioimaging. *Chemistry* **20**, 1010–1016.
55. Sen, N., Paul, B.D., Gadalla, M.M., Mustafa, A.K., Sen, T., Xu, R., Kim, S., and Snyder, S.H. (2012). Hydrogen sulfide-linked sulfhydration of NF- κ B mediates its antiapoptotic actions. *Mol. Cell* **45**, 13–24.
56. Chi, H., Liu, C., Yang, H., Zeng, W.F., Wu, L., Zhou, W.J., Wang, R.M., Niu, X.N., Ding, Y.H., Zhang, Y., et al. (2018). Comprehensive identification of peptides in tandem mass spectra using an efficient open search engine. Published online October 8, 2018. *Nat. Biotechnol.*
57. Lu, A., Li, H., Niu, J., Wu, S., Xue, G., Yao, X., Guo, Q., Wan, N., Abliz, P., Yang, G., et al. (2017). Hyperactivation of the nlrp3 inflammasome in myeloid cells leads to severe organ damage in experimental lupus. *J. Immunol.* **198**, 1119–1129.
58. Kölling, M., Kaucsar, T., Schauerer, C., Hübner, A., Dettling, A., Park, J.K., Busch, M., Wulff, X., Meier, M., Scherf, K., et al. (2017). Therapeutic mir-21 silencing ameliorates diabetic kidney disease in mice. *Mol. Ther.* **25**, 165–180.

STAR★METHODS

KEY RESOURCES TABLE

REAGENT or RESOURCE	SOURCE	IDENTIFIER
Antibodies		
APC anti-mouse CD3	Biolegend	Cat#100236; RRID: AB_2561456
Percp-Cy5.5 anti-mouse CD4	Biolegend	Cat#116012; RRID: AB_2563023
PE anti-mouse CD44	Biolegend	Cat#103023; RRID: AB_493686
Pacific Blue anti-mouse CD45	Biolegend	Cat#103126; RRID: AB_493535
APC/Fire™ 750 anti-mouse CD62L	Biolegend	Cat#104449; RRID: AB_2629771
FITC anti-mouse IFN- γ	Biolegend	Cat#505806; RRID: AB_315400
PE anti-mouse IL4	Biolegend	Cat#504104; RRID: AB_315318
PE anti-mouse IL17	Biolegend	Cat#506904; RRID: AB_315464
PE anti-mouse Foxp3	Biolegend	Cat#126404; RRID: AB_1089117
FITC anti-Annexin V	Biolegend	Cat#640906; RRID: AB_2561291
PE-Cy7 anti-7AAD	BD Biosciences	Cat#559925; RRID: AB_2869266
Alexa Fluor™ 568 goat anti-rat IgG(H+L)	Invitrogen	Cat#A11077; RRID: AB_2534121
Alexa Fluor™ 488 goat anti-rat IgG(H+L)	Invitrogen	Cat#A11006; RRID: AB_2534074
Alexa Fluor™ 568 goat anti-rabbit IgG(H+L)	Invitrogen	Cat#A11036; RRID: AB_10563566
Alexa Fluor™ 488 goat anti-rabbit IgG(H+L)	Invitrogen	Cat#A11008; RRID: AB_143165
Alexa Fluor™ 568 goat anti-mouse IgG(H+L)	Invitrogen	Cat#A11004; RRID: AB_2534072
Alexa Fluor™ 488 goat anti-mouse IgG(H+L)	Invitrogen	Cat#A11001; RRID: AB_2534069
Alexa Fluor™ 568 rabbit anti-goat IgG(H+L)	Invitrogen	Cat#A11079; RRID: AB_2534123
Alexa Fluor™ 488 donkey anti-goat IgG(H+L)	Invitrogen	Cat#A11055; RRID: AB_2534102
Anti-CBS-rab	CST	Cat#14782S; RRID: AB_2798609
Anti-CSE-rab	Abcam	Cat#ab136604; RRID: AB_2722603
Anti-3-MST-rab	cloud-clone	Cat#PAC625Hu01; RRID: AB_3065106
Anti-FLAG-mouse	Servicebio	Cat#GB12938; RRID: AB_3065118
Anti-GAPDH-rab	CST	Cat#5174S; RRID: AB_10622025
Anti-p-STAT1	CST	Cat#7649S; RRID: AB_10950970
Anti-STAT1	CST	Cat#14994S; RRID: AB_2799965
Anti-p-STAT3	CST	Cat#9145; RRID: AB_2491009
Anti-STAT3	CST	Cat#12640; RRID: AB_2629499
Anti-STAT4	CST	Cat#2653; RRID: AB_2255156
Anti-STAT5	CST	Cat#25656; RRID: AB_2798908
Anti-Sep15	Abcam	Cat#ab124840; RRID: AB_10972510
Anti-CD63	Santa	Cat#sc-5275; RRID: AB_627877
Anti-CD81	Santa	Cat#sc-70803; RRID: AB_1120720
Anti-TSG101	Abcam	Cat#ab125011; RID: AB_10974262
Anti-Alix	Abcam	Cat#ab275377; RRID: AB_2943044
Anti-Cleaved-caspase 3	CST	Cat#9664s; RRID: AB_2070042
Chemicals, peptides, And recombinant proteins		
Purified anti-mouse CD3	Biolegend	Cat#100340
Purified anti-mouse CD28	Biolegend	Cat#102116
Anti-IL-4 antibody	BioXCell	Cat#BE0045
Anti-IFN γ antibody	BioXCell	Cat#BE0055
Recombinant Murine IL-6	R&D	Cat#406-ML-005
Recombinant Murine IL-23	R&D	Cat#1887-ML-010
Recombinant Murine IL-1 β	PeproTech	Cat#211-11B

(Continued on next page)

Continued

REAGENT or RESOURCE	SOURCE	IDENTIFIER
Recombinant Human TGF- β	PeproTech	Cat#100-21
NaHS	Aladdin	Cat#S106641
HA	Sigma	C#379921
PAG	Sigma	Cat#P7888
PLP	Sigma	Cat#P9255
L-cystine	Sigma	Cat#C7352
WSP-5	MKBio	Cat#MX5302
STS	Enzo	Cat#ALX-380-014
Z-VAD	MCE	Cat#HY-16658
PMA	Sigma	Cat#524400
Ionomycin	Sigma	Cat#407952
Monensin	BD Biosciences	Cat#554724
Alexa Fluor® 488 C5 maleimide	Invitrogen	Cat#A10254
DTT	Invitrogen	Cat#D1532
Iodoacetamide	Sigma	Cat#I1149
IPM probe	KeraFast	Cat#EVU111
Light UV-cleavable azido-biotin	KeraFast	Cat#EVU102
Heavy UV-cleavable azido-biotin	KeraFast	Cat#EVU151
Critical commercial assays		
Zombie Aqua™ Fixable Viability Kit	Biolegend	Cat#423101
FoxP3/transcription factor staining kit	Thermo Fisher	Cat#00-5523-00
PE Annexin V Apoptosis Detection Kit	BD Biosciences	Cat#559763
10X Annexin V Binding Buffer	BD Biosciences	Cat#556454
Mouse Naïve CD4 ⁺ T Cell Isolation Kit	Miltenyi Biotec	Cat#130-104-453
Pierce MS-Compatible Magnetic IP Kit	Sigma	Cat#90409
CFSE Cell Division Tracker Kit	Biolegend	Cat#423801
DeadEnd™ Fluorometric TUNEL kit	Promega	Cat#G3250
Mouse ANA ELISA Kit	MEIMIAN	Cat#MM-1042M
Mouse BUN ELISA Kit	MEIMIAN	Cat#MM-0692M
Mouse IgG ELISA Kit	MEIMIAN	Cat#MM-0057M
Mouse IgM ELISA Kit	MEIMIAN	Cat#MM-0058M
Deposited data		
Unprocessed raw data	DataS1	N/A
Other data (proteomics, low-pH QTRP)	Mendeley	https://doi.org/10.17632/tzpytt8vzj.1
Experimental models: Mouse Strain		
Mouse: B6.MRL-Fas ^{lpr} /J (MRL/lpr mice)	Jackson Laboratories	Cat#000482
B6.129S1-Bcl2l1tm1.1Ast/J (Bim ^{-/-} mice)	Jackson Laboratories	Cat#004525
Oligonucleotides		
qRT-PCR primers see Table S3	This paper	N/A
Point mutant constructs primer see Table S4	This paper	N/A
Software and algorithms		
Prism 9.0	GraphPad	https://www.graphpad.com/
ImageJ	ImageJ	https://imagej.net/ij/
NovoCyte software ⁴	Agilent Technologies	https://www.agilent.com.cn
Other		
ChemiDoc™ MP imaging system	BioRad	N/A
NovoCyte flow cytometer	Agilent Technologies	N/A
Transmission electron microscopy	FEI Company	N/A
Elyra 7 Lattice SIM	Zeiss	N/A
H2S microelectrode sensor	Unisense	N/A

RESOURCE AVAILABILITY

Lead contact

Further information and requests for resources and reagents should be directed to and will be fulfilled by the lead contact, Songtao Shi (shisiongtao@mail.sysu.edu.cn).

Material availability

Plasmids, cell lines and other materials generated in this study are available upon reasonable request to the [lead contact](#).

Data and code availability

- Original data for creating all graphs in the paper are provided in [Data S1](#).
- This paper does not report original code.
- Any additional information required to reanalyze the data reported in this paper is available from the [lead contact](#) upon reasonable request.

EXPERIMENTAL MODEL AND SUBJECT DETAILS

Animals

B6.MRL-Fas^{lpr}/J (MRL/lpr mice, JAX, #000482) and B6.129S1-Bcl2l1^{1tm1.1Ast}/J (Bim^{-/-} mice, JAX, #004525) mice were purchased from Jackson Lab. B6;129S-Ct^{tm1(Luc)Smoc} (CSE^{-/-}, NM-KI-00004, Shanghai Model Organisms Center, China) mice were a gift from Professor Bin Geng (Chinese Academy of Medical Sciences). B6.129P2-Cb^{stm1}Unc/J (CBS^{-/-}, JAX, #002461) mice were a gift from Professor YingHong Shi (Fudan University). Selenoprotein F knockout (Sep15^{-/-}) mice were a gift from Professor Jing Tian (Shenzhen University). The symptoms in the mice of SLE showed significant gender differences. The onset of SLE in female patients and female mice was earlier than that in males.⁴⁹ In order to avoid the influence of gender differences on the experimental results, female mice (12–16 weeks) were used in this study. All animal experiments were approved by the Animal Ethical and Welfare Committee of Sun Yat-Sen University (SYSU-IACUC-2023-000441).

Antibodies and reagents

All antibodies, cytokines, kits, and other resources used in this study are listed in [key resource table](#).

METHOD DETAILS

Apoptosis modulation

For apoptotic rate analysis *in vivo*, STS (120 ng/kg body weight) was intraperitoneally (*i.p.*) administered to mice twice a week for 4 weeks as reported previously.¹⁹ For apoptotic inhibition, Z-VAD (3.3 mg/kg body weight) was *i.p.* administered to mice for 1 h before STS treatment.⁵⁰ For *in vitro* apoptotic induction, STS and UV were used to induce apoptosis of mBMSCs, PBMCs and CD4⁺ T cells. PBMCs and CD4⁺ T cells were treated with 250 nM STS for 6 h at 37°C, while mBMSCs were treated with 250 nM STS for 10 h. In UV induction, PBMCs and CD4⁺ T cells were treated with 150 mJ/cm⁻² UV-C irradiation (Stratalinker) for 4 h, while mBMSCs were treated with UV-C irradiation for 6 h. In apoptosis inhibition assays, all cells were incubated for 1 h with 50 μM Z-VAD before stimulation with STS or UV.

Injection of H₂S donor and inhibitor

H₂S donor NaHS (5 mg/kg body weight), and CBS inhibitor HA (3 mg/kg body weight) and CSE inhibitor PAG (3 mg/kg body weight) were *i.p.* administered into mice twice a week. After 4 weeks, samples were harvested and analyzed.^{13,21}

Isolation of mBMSCs

Bone marrow cells were flushed out from the bone marrow of femurs with 5% fetal bovine serum (FBS; Gibco BRL, NY, USA) in PBS. Single-cell suspension was obtained by passing through 70 μm cell strainer (BD Biosciences, CA, USA). Cells were incubated for 48 h at 37°C in 5% CO₂. The nonadherent cells were washed out with PBS and mBMSCs were cultured for 10 days with alpha minimum essential medium (α-MEM, Gibco BRL) supplemented with 10% FBS, 2 mM L-glutamine (Gibco BRL), 50 μM 2-mercaptoethanol (Gibco BRL), 100 U/ml penicillin and 100 μg/ml streptomycin (Gibco BRL). CBS^{-/-} mBMSCs and CSE^{-/-} mBMSCs were isolated from CBS^{-/-} mice and CSE^{-/-} mice, respectively.

Isolation of apoVs

mBMSCs were incubated with STS (250 nM) to induce apoptosis. Sequential centrifugation (800 g for 10 mins, 2,000 g for 10 mins, and 16,000 g for 30 mins) was conducted to separate apoVs. ApoVs were characterized by transmission electron microscopy (TEM; FEI Company, MA, USA), western blotting and ZetaView instrument (Particle Metrix, Ammersee, Germany) as previously reported.⁵¹

CBS^{-/-} apoVs, CSE^{-/-} apoVs and si-3-MST apoVs were isolated from CBS^{-/-} mBMSCs, CSE^{-/-} mBMSCs and si-3-MST mBMSCs, respectively. Exosomes from mBMSCs were collected to compare with apoVs as described previously.²⁰

Immunofluorescence staining of apoVs

ApoVs were resuspended and blocked with 5% bovine serum albumin (BSA) in PBS for 1 h. Then apoVs were incubated with anti-CBS, anti-CSE, and anti-3-MST antibody overnight at 4°C, respectively. After incubation, the samples were washed with PBS three times, and followed by differential centrifugation. ApoVs were incubated in secondary antibody for 1 h at 37°C and subsequently incubated with membrane dye CellMask DeepRed and Annexin V for 30 mins at 37°C. ApoVs were analyzed by Elyra 7 Lattice SIM (Zeiss, Jena, Germany).

Th17 cell differentiation

Naïve CD4⁺ T cells (CD4⁺CD25⁻CD44^{low}CD62L^{high}) were isolated from the spleen by negative selection using the mouse naïve CD4⁺ T cell isolation Kit (Miltenyi Biotec, Bergisch Gladbach, Germany) according to the manufacturer's protocol. Cells were activated with plate-bound anti-mouse CD3 (2 µg/ml) and anti-mouse CD28 (2 µg/ml) in RPMI 1640 medium supplemented with 10% FBS, 1 mM L-glutamine and 50 µM 2-mercaptoethanol, 100 U/ml penicillin and 100 µg/ml streptomycin. For Th17 cell differentiation, IL-1β (10 ng/ml), IL-6 (20 ng/ml), IL-23 (10 ng/ml), TGFβ (1 ng/ml), anti-mouse IL-4 (5 µg/ml) and anti-mouse IFNγ (10 µg/ml) were added to cell cultures.⁵² Cells were supplemented with fresh media on day 3 and analyzed on day 5.

Flow cytometry

For intracellular cytokine staining, cells were stimulated with phorbol 12-myristate 13-acetate (PMA, 50 ng/mL), ionomycin (1 mg/mL) and monensin (GolgiStop; 1 mg/mL) for 4 h. After staining for surface markers, cells were permeabilized with a FoxP3/transcription factor staining kit (Thermo Fisher, CA, USA) and intracellularly stained for corresponding antibodies. The labelled antibodies include: APC anti-mouse CD4, FITC anti-mouse IFN-γ, PE anti-mouse IL-4, PE anti-mouse IL-17, PE anti-mouse Foxp3. For apoptotic rate assay, cells were stained with FITC anti-Annexin V and PE-Cy7 anti-7AAD for 15 mins at room temperature. Then cells were analyzed by flow cytometry (NovoCyt, Agilent Technologies, CA, USA).

H₂S microelectrode detection method

Cell supernatants and blood were collected into a temperature-controlled micro-respiration chamber (Unisense, Aarhus, Denmark) to measure H₂S concentration via H₂S microelectrode sensor (Model H₂S-MRCh; Unisense) coupled with a Unisense PA2000 amplifier.

Lead sulfide detection method

H₂S from tissue and blood were detected using the lead acetate/lead sulfide method.⁵³ Briefly, fresh tissue was collected and homogenized. Protein concentration was analyzed with BCA assay. Then, a reaction mixture was prepared with L-cysteine (10 mM) and Pyridoxal 5'-phosphate hydrate (PLP; 1 mM). Protein (100 mg) from each sample or plasma (20 µL) was added to the reaction mixture in a 96-well plate. The plate was overlaid with lead acetate paper and incubated at 37°C until lead acetate was detected.

H₂S probe staining

Endogenous H₂S production of cells and apoVs was detected by Washington State Probe-5 (WSP-5), which is based on the dual-nucleophilicity of H₂S and selectively reacted with H₂S to generate a green fluorescence signal.⁵⁴ Cells and apoVs were cultured with WSP-5 for 30 mins and washed with PBS three times. The fluorescent of WSP-5 was detected by confocal microscopy.

Western blotting

Co-IP test was performed using Pierce MS-Compatible Magnetic IP Kit. Briefly, cell lysates were incubated with antibody at 4°C overnight, followed by incubation with protein A/G magnetic beads for 2 h. After washing five times, the precipitates were eluted for immunoblotting and mass spectrometric detection. Western blotting was performed as previously described.⁵¹ Total protein was extracted with a total protein extraction kit (Thermo Fisher) following the manufacturer's protocol. Nuclear protein and cytoplasm protein were extracted with nuclear and cytoplasmic protein extraction kit (Beyotime, Beijing, China). For western blotting, 20 µg protein was used for electrophoresis and transferred to PVDF membranes (Millipore, Billerica, MA, USA). After blocking for 1 h, the membranes were incubated with corresponding primary antibody at 4°C overnight, and incubated with HRP-conjugated secondary antibodies for 1 h. Lastly, the membranes were visualized by SuperSignal West Pico Chemiluminescent Substrate (Thermo Fisher) and scanned by ChemiDoc™ MP imaging system (Bio-Rad, CA, USA).

Quantitative PCR analysis

Total RNA was extracted from cells and tissues using TRIzol reagent (Life Technologies, MD, USA) and cDNA was synthesized using a reverse transcriptase M-MLV Kit (TaKaRa, Tokyo, Japan). Gene expression levels were quantified by RT-PCR using a SYBR Green kit (Roche, Basel, Switzerland) with gene-specific primers (Table S3).

Sulfhydrylation assay using maleimide

This assay was designed as previously described.⁵⁵ Cell lysates were collected and incubated with Alexa Fluor® 488 C5 maleimide (10 μ M) at 4°C for 2 h. For total protein sulfhydrylation assay, cell lysates were treated with or without DTT (1 mM) at 4°C for 1 h. After boiling at 95°C for 10 mins, the samples were used for electrophoresis and transferred to PVDF membranes for western blotting analysis. For specific protein sulfhydrylation assay, the primary antibody was added to cell lysates and incubated overnight at 4°C; IgG was used as control. Protein A/G magnetic beads were added at 4°C for 2 h. Immunoprecipitates were collected after centrifugation at 2,500 rpm at 4°C for 5 mins. The beads were pelleted and washed, and then treated with or without DTT (1 mM) at 4°C for 1 h. The samples were boiled and used for electrophoresis, and then scanned with imaging system.

Click chemistry for H₂S-mediated sulfhydrylation proteomics

Th17 cells were treated by NaHS and lysed with lysis buffer. Cell lysates were labeled with the 2-iodo-N-(prop-2-yn-1-yl) acetamide (IPM; 100 μ M) probe at room temperature for 1 h in the dark. Probe-labeled proteome samples (pH 5.0) were alkylated by adding the stock solution of iodoacetamide (40 mM). Samples were resuspended in 50 mM ammonium bicarbonate by sonication. 2 mg protein was used and digested with sequencing grade trypsin (Promega, WI, USA) at a 1:50 (enzyme/substrate) ratio overnight at 37°C. The tryptic digests were desalted with HLB extraction cartridges (Waters, MA, USA), and evaporated to dryness. Click chemistry was performed by the addition of 1 mM light (NaHS group) or heavy (Control group) UV-cleavable azido-biotin for 2 h. Light and heavy isotopic tagged samples were mixed at a ratio of 1:1 after click chemistry. Samples were enriched with streptavidin-sepharose beads (GE, MA, USA) and irradiated with 365-nm UV light. The supernatant was collected and stored at -20°C until LC-MS/MS analysis. Quantification of light to heavy ratios (RL/H) was performed using pQuant and RL/H < 0.6 was considered to be true identifications.

LC-MS/MS analysis

Mass spectrometry was performed on Orbitrap Q Exactive HF-X mass spectrometer coupled with an UltiMate 3000 LC system (Thermo Fisher). Samples were reconstituted in formic acid and transferred into precolumn, and then the precolumn was connected to a microcapillary analytical column. HCD MS/MS spectra were recorded in data-dependent mode using the top-20 method. Raw data files were searched against the *Mus musculus* UniProt canonical database with pFind 3.0 studio (<http://pfind.ict.ac.cn/software/pFind3/index.html>).⁵⁶

Generation of site mutant construct

Sep15, PKM and Nfkb1 expression construct (Miaolingbio, Wuhan, China) were used as templates to generate site mutant construct according to the results of sulfhydrylation proteomics (Sep15^{C38A}, PKM^{C49A}, Nfkb1^{C159A}) using a Fast Site-Directed Mutagenesis Kit (Tiangen, Beijing, China). The mutant clone was confirmed by DNA sequencing. The primers used to generate point mutant constructs were as follows (Table S4).

RNA-Mediated Interference and Plasmid Transfection

P3 Primary Cell 4D-Nucleofector™ kit was used for knockdown of STAT1 via siRNA and site mutant construct in CD4⁺ cells according to the manufacturer's instructions (Lonza, Basel, Switzerland). Naïve CD4⁺ T cells were stimulated with anti-CD3 and anti-CD28 and were transduced by electroporation with siRNA or plasmid (10 nM), and cells were cultured and stimulated for further experiments.

Histology

Renal tissues from different groups were fixed in 10% buffered formalin or cryopreserved in optimal cutting temperature (OCT) compound. Paraffin sections were prepared and stained with H&E and PAS for renal damage evaluation. In H&E staining, the pathological score was ranged from 0 to 4: 0, normal; 1, a small increase in cells in the glomerular mesangium; 2, a larger number of cells in the mesangium; 3, glomerular lobular formation and thickened basement membrane; and 4, glomerular crescent formation, sclerosis, tubular atrophy, and casts. The score for each animal was calculated by dividing the total score for the number of glomeruli observed.⁵⁷ PAS staining was used to evaluate mesangial expansion by mesangial index (MI).⁵⁸ The MI value was calculated by PAS⁺ area (pixel) of glomerulus / total area (pixel) of glomerulus.

For IgG deposition evaluation, frozen renal and skin tissue sections were prepared and stained with Alexa Fluor 488-conjugated anti-mouse IgG. For tissue apoptotic rate analysis, frozen spleen tissue sections from different groups were prepared and stained with DeadEnd™ Fluorometric TUNEL kit (Promega).

QUANTIFICATION AND STATISTICAL ANALYSIS

Normal distribution was assessed using the Shapiro-Wilk test. Comparisons between two groups were analyzed using independent unpaired two-tailed Student's t tests for normally distributed data. Comparisons between more than two groups were analyzed using one-way ANOVA with Tukey's test. *P* values less than 0.05 were considered statistically significant.